Interactions of the iron and phosphorus cycles: A three-dimensional model study

S. Dutkiewicz, M. J. Follows, and P. Parekh

Department of Earth, Atmospheric and Planetary Sciences, Massachusetts Institute of Technology, Cambridge, Massachusetts, USA

Received 16 July 2004; revised 21 December 2004; accepted 2 February 2005; published 16 March 2005.

[1] We use an ocean circulation, biogeochemistry, and ecosystem model to explore the interactions between ocean circulation, macro- and micro-nutrient supply to the euphotic layer, and biological productivity. The model suggests a tight coupling between the degree of iron limitation in the upwelling subpolar and tropical oceans and the productivity of the adjacent subtropical gyres. This coupling is facilitated by lateral Ekman transfer of macro-nutrients in the surface ocean. We describe a coarse resolution configuration of the MIT ocean circulation and biogeochemistry model in which there are fully prognostic representations of the oceanic cycles of phosphorus, iron, and silicon. The pelagic ecosystem is represented using two functional groups of phytoplankton and a single grazer. Using present-day forcing, the model qualitatively captures the observed basin and gyre scale patterns of nutrient distributions and productivity. In a suite of sensitivity studies we find significant regional variations in response to changes in the aeolian iron supply. In a dustier (model) world, the Southern Ocean and Indo-Pacific upwelling regions are more productive, but there is a decrease in productivity in the subtropical gyres and throughout the Atlantic basin. These results can be described most easily by a simple conceptual classification of the Southern and Indo-Pacific oceans into two regimes: (1) upwelling, iron limited regions and (2) macro-nutrient limited, oligotrophic subtropical gyres. Enhancing the aeolian iron supply to the upwelling regions relieves iron limitation and increases local primary and export production, but reduces the Ekman transfer of phosphate to the neighboring subtropical gyres. Consequently, over time, the gyres become further depleted in macro-nutrients and productivity decreases in response to global scale iron fertilization. In a large-scale analogy, the macro-nutrient budget of the Atlantic is maintained by lateral transfer of nutrients in the upper ocean. Enhanced aeolian supply of iron leads to increased productivity in the Southern Ocean and Indo-Pacific upwelling regions, reducing the lateral transfer of macro-nutrients to the Atlantic basin, which becomes increasingly macro-nutrient limited throughout.

Citation: Dutkiewicz, S., M. J. Follows, and P. Parekh (2005), Interactions of the iron and phosphorus cycles: A three-dimensional model study, *Global Biogeochem. Cycles*, *19*, GB1021, doi:10.1029/2004GB002342.

1. Introduction

[2] What regulates the patterns and rates of primary and export production in the ocean? It has long been clear that the availability of macro-nutrients (nitrate and phosphate) at the surface ocean is a key factor, and that the major supply of these nutrients to the euphotic zone is upwelling or entrainment from the deeper ocean. Since the near-surface vertical motions on the gyre scale are dominated by Ekman pumping, there is a clear and simple relationship between the wind stress curl, upwelling of macro-nutrients to the surface, and chlorophyll: Upwelling regions have high macro-nutrient supply and high chlorophyll, and downwelling subtropical gyres have a scarcity of both macro-nutrients and chlorophyll. This simple view is modified in the so-called High Nitrate Low Chlorophyll regimes (HNLC): upwelling regions where surface macro-nutrients remain under-utilized and chlorophyll concentrations are lower than might otherwise be expected. While light limitation and differences in community structure are possible explanations [e.g., *Popova et al.*, 2000; *Fasham*, 1995; *Banse*, 1992], it is now clear that iron is a key limiting nutrient, regulating productivity, in large areas of the oceans [*Martin and Fitzwater*, 1988; *Coale et al.*, 1996; *Martin et al.*, 1994]. Hence the simple, zero-order relationship between (broad-scale) upwelling and chlorophyll is modulated by the availability of iron.

[3] Here, in the context of an ocean circulation and biogeochemistry model, we examine the interactions be-

0886-6236/05/2004GB002342$12.00

tween a macro-nutrient (phosphorus), a micro-nutrient (iron), and the pelagic ecosystem which set the regional expression of surface chlorophyll and patterns of productivity. Iron and phosphate are decoupled in the interior of the ocean due to scavenging and complexation processes which act on iron, but not macro-nutrients [e.g., *Johnson et al.*, 1997; *Archer and Johnson*, 2000; *Parekh et al.*, 2004] (also P. Parekh et al., Decoupling of iron and phosphate in the global ocean, submitted to *Global Biogeochemical Cycles*, 2005) (hereinafter referred to as Parekh et al., submitted manuscript, 2005). Both are supplied through the remineralization of sinking organic matter, but iron is also scavenged onto sinking particles. This results in upwelling waters being iron deficient relative to the supply of phosphate. A significant fraction of the upper ocean supply of iron comes from aeolian dust. However, regions of high dust deposition do not coincide with regions of high upwelling in many regions of the ocean.

[4] Ice core records suggest an anti-phase relationship between high pCO_2 and low dust during the past several hundred thousand years [*Petit et al.*, 1999; *Martin*, 1990]. This suggests some link, if not control, of dust on atmospheric CO_2. We need a better understanding of how changes to the aeolian dust supply affects the ocean pelagic ecosystem. What might be the consequences of potential future changes in the aeolian iron supply?

[5] Our aim here is to sketch, and illustrate, a conceptual view of the coupling and interplay between phosphorus and iron cycles and the implications for regional and global ocean productivity. We seek to provide a framework with which to understand how the coupling and decoupling of these elemental cycles through biological, chemical, and physical processes control the patterns of global surface ocean productivity, and its response to changes in the aeolian supply of iron.

[6] In this paper, we argue that the modern ocean can be described in terms of several nutrient/productivity regimes: (1) downwelling, macro-nutrient limited subtropical gyres; (2) HNLC upwelling regions in the Southern Ocean and Indo-Pacific basin; and (3) high productivity, macro-nutrient limited upwelling regions in the Atlantic basin. We also argue that these regions are intimately linked, and that by changing productivity in the upwelling regions, we regulate the supply of macro-nutrients to the subtropical gyres.

[7] We illustrate this conceptual view and investigate the links between these regions with a numerical model of the coupled oceanic cycles of iron, phosphorus, and silicon which incorporates an explicit representation of the pelagic ecosystem. Here we do not try to include a fully comprehensive biogeochemical model, but to include the aspects most relevant to illustrate the concepts of interest (the interplay of phosphate and iron cycles). In section 2 we describe the numerical model, and in section 3 we describe its mean state after several thousand years of spinup in a modern ocean configuration. We demonstrate that this model, in a coarse resolution configuration, qualitatively captures the broad features of the modern ocean distributions of each of the three nutrients and the patterns of chlorophyll concentrations. In section 4 we discuss sensitivity studies with the model which illustrate how the coupling of phosphorus and iron cycles regulates the productivity in the subpolar and subtropical (upwelling, downwelling) regions and the contrasting regimes of the Atlantic and Pacific basins.

2. A Global Circulation, Biogeochemistry, and Ecosystem Model

[8] We employ an ecosystem model of intermediate complexity, embedded in a three-dimensional ocean circulation model. The model represents the coupled cycles of phosphorus, silicon, and iron, and incorporates an explicit representation of the pelagic ecosystem with two "functional groups" of phytoplankton: nominally diatoms and "small" phytoplankton. The iron cycle model includes explicit account of scavenging onto sinking particles and complexation with organic ligands. The iron parameterization has been developed and applied in simpler biogeochemical models [*Parekh et al.*, 2004; submitted manuscript, 2005].

[9] While not as complex as some recent global models [e.g., *Aumont et al.*, 2003; *Gregg et al.*, 2003], our coupled physical-ecosystem model does capture the basic features of the ocean pelagic system. The nutrient cycles in this model are fully prognostic over the whole water column, and we may conduct sensitivity studies exploring the relationships and coupling between those nutrient cycles and the representation of surface ocean ecology. In particular, we examine the model's response to changes in aeolian dust deposition. What happens if the iron limitation is relieved in HNLC regions? Also, what happens when regions which are currently iron replete become iron starved? Will this drastically affect ocean productivity and macro-nutrient distribution? We use our model and these sensitivity experiments as a tool to develop a conceptual three-dimensional view of nutrient supply and the interplay of phosphate and iron cycles in the ocean. While our model is still limited in its description of the ecosystem and unresolved features of the circulation, we believe that it is a useful tool for a qualitative exploration of the interplay of macro-nutrients and iron, aeolian dust supply, and ocean circulation. We note that this study is still somewhat idealized in nature, and we do not attempt to represent the more complex nitrogen cycle.

2.1. Physical Model

[10] We use the MIT general circulation model [*Marshall et al.*, 1997a, 1997b] in a coarse resolution global configuration ($2.8^\circ \times 2.8^\circ$, 15 vertical levels). The effects of unresolved mesoscale eddy transports are represented by the *Gent and McWilliams* [1990] parameterization with isopycnal mixing coefficient of 1×10^3 m^2 s^{-1}. We impose a uniform vertical viscosity of 1×10^{-3} m^2 s^{-1} and vertical diffusion of 5×10^{-5} m^2 s^{-1} for all tracers. The model is integrated asynchronously, with momentum and tracer time steps of 900 s and 12 hours, respectively. The bathymetry, though coarse, is realistic but has a closed boundary at 80°N, and the Arctic Ocean is not represented. The physical model is forced with climatological annual cycles of wind [*Trenberth et al.*, 1989] and heat and freshwater fluxes

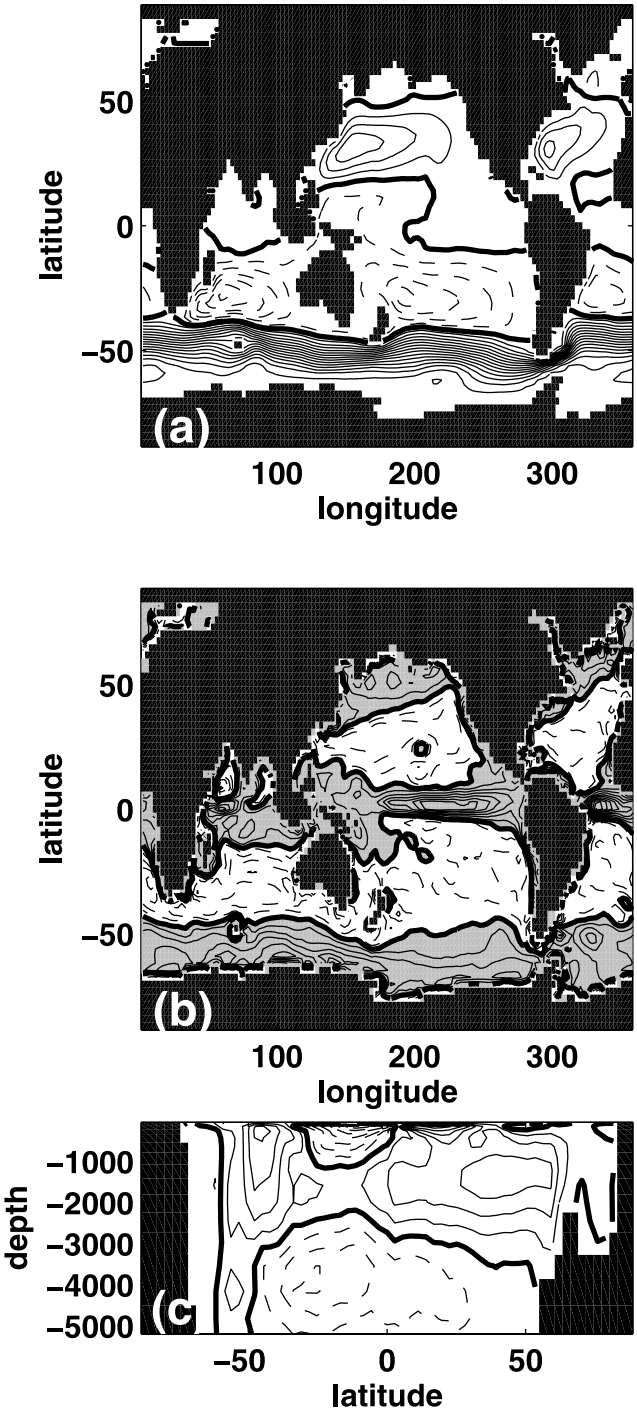

Figure 1. General circulation model. (a) Barotropic stream function (Sv). (b) Vertical velocity at 50 m (m yr^{-1}). (c) Global zonally averaged residual overturning circulation (Sv). Heavy contour denotes zero, and dashed contours denote negative values. Contour intervals are 10 Sv for Figure 1a, 20 m yr^{-1} for Figure 1b, and 5 Sv for Figure 1c. Shading in Figure 1b denotes upwelling regions.

[*Jiang et al.*, 1999]. Sea-surface temperature and salinity are also restored toward monthly climatologies [*Levitus and Boyer*, 1994; *Levitus et al.*, 1994] with timescales of 2 months and 1 year, respectively. The model configuration is generally similar to that applied in the Ocean Carbon-cycle Model Intercomparison Studies (OCMIP) [e.g., *Dutay et al.*, 2002; *Matsumoto et al.*, 2004], but here different surface boundary conditions have been applied with some improvements to the circulation (for example, a greater volume flux and residual overturning in the region of the Antarctic Circumpolar Current). The physical model is spun up for 5000 years. In Figure 1 we show the barotropic stream function, "residual" overturning (which includes the effect of eddies) and the vertical velocity at 50 m. The model qualitatively captures the major current systems and quiescent subtropical gyres and patterns of upwelling and downwelling. The maximum overturning circulation in the Northern Hemisphere is about 17 Sv (comparable to the 15 ± 2 Sv estimated by *Ganachaud and Wunsch*, 2000), representing the deep water formation in the North Atlantic Ocean. The zonally averaged, residual overturning in the Southern Ocean reaches about 22 Sv, which, based on diagnostics from observed transient tracers, is perhaps a little higher than in the ocean [*Ito et al.*, 2004].

2.2. Nutrient Cycles

[11] We explicitly represent the coupled cycles of phosphorus, silicon, and iron. Phosphorus and silicon are assumed to have oceanic residence times much longer than the oceanic turnover timescale. Their global average oceanic concentration is fixed, riverine and atmospheric sources are

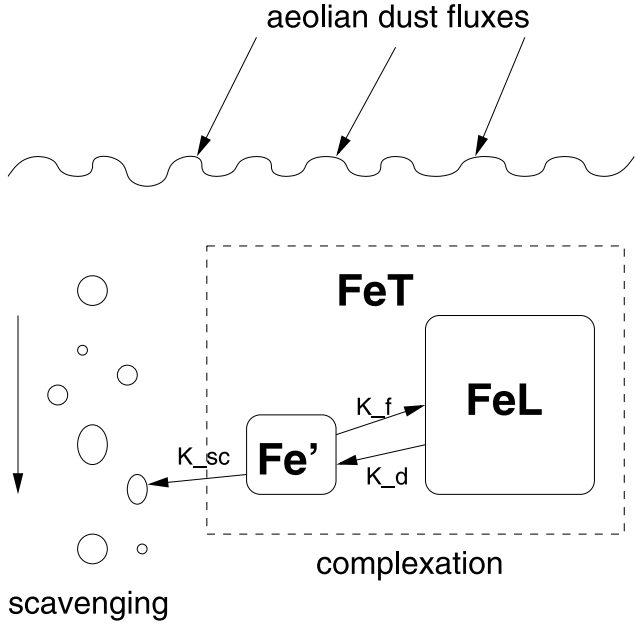

Figure 2. Schematic of iron cycle parameterization following *Parekh et al.* [2004], showing the source through aeolian dust deposition, the sink due to scavenging of free iron onto sinking particles, and complexation with an organic ligand. Symbols are: Fe′ (free iron), FeL (complexed form of iron), FeT (total iron, Fe′+ FeL), K_{sc} (scavenging rate), K_f (complexation forward rate constant), and K_d (complexation reverse rate constant).

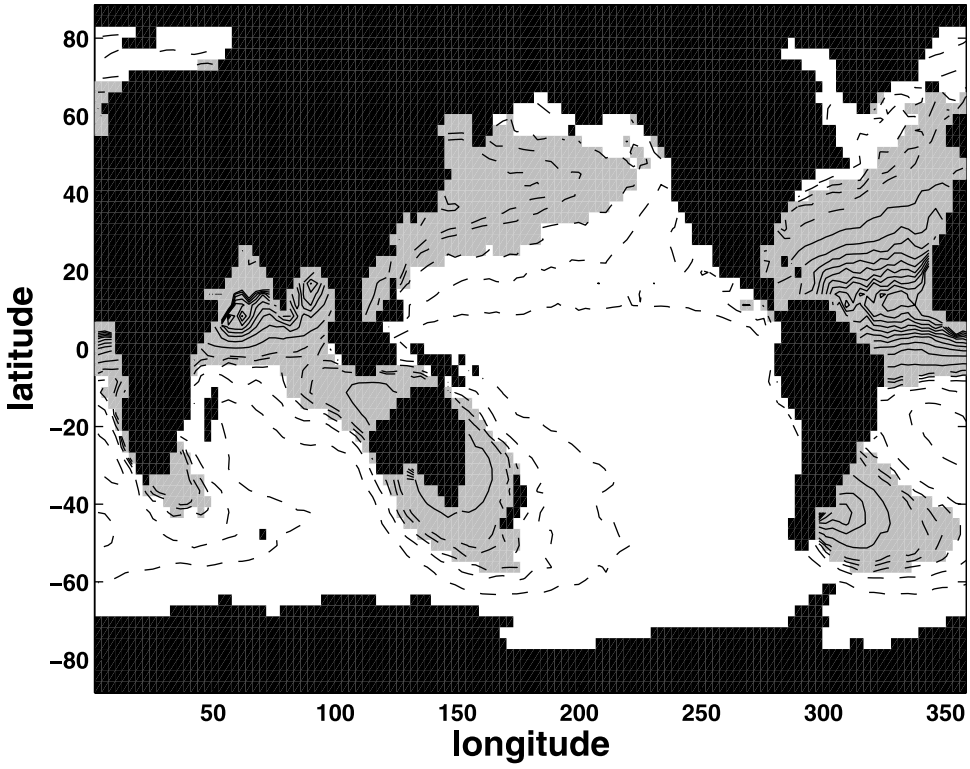

Figure 3. Annual mean aeolian iron deposition (mmol Fe m^{-2} yr^{-1}) determined from modeled dust deposition of *Mahowald et al.* [2003] and assuming 3.5% iron by weight. Dashed contour interval is 0.1 from 0 to 0.5 mmol Fe m^{-2} yr^{-1}. Solid contours are every 1 mmol Fe m^{-2} yr^{-1}. Shaded areas have iron flux above 0.3 mmol Fe m^{-2} yr^{-1}.

not represented, and sedimentation is not allowed. In contrast, iron has a relatively short residence time in the ocean (estimated to be between 70 and 200 years [*Bruland et al.*, 1994; Parekh et al., submitted manuscript, 2005], so we do not impose fixed total global iron concentrations. However, the sources and sinks (discussed below) do come into dynamic balance when the model reaches a steady state.

[12] These three nutrients are consumed during photosynthesis in the explicit ecosystem (described in section 2.3) and exported to the disphotic zone as particulate or dissolved organic matter. Some fraction is also simply subducted as unutilized dissolved inorganic (or preformed) nutrients. The model of *Aumont et al.* [2003] considers the same elements; the more complex models of *Moore et al.* [2002a] and *Gregg et al.* [2003] also include nitrogen. Here, for clarity, we do not represent the additional complexities of the nitrogen cycle. We recognize that this can be a very important limiting element, but believe that the concepts presented here are not qualitatively dependent on its representation.

[13] In addition to uptake during photosynthesis and remineralization, iron also has other sources and sinks in the water column (see Figure 2). The sources include aeolian dust deposition [*Duce and Tindale*, 1991], shelf sediments [*Elrod et al.*, 2004], riverine inputs, and hydrothermal activity. Here we impose only an aeolian source, depicted in Figure 3, based on modeled dust deposition estimates of *Mahowald et al.* [2003] and assuming that 3.5% of the dust weight is iron. The strongest deposition occurs downwind of the major deserts. Hence the remote Southern Ocean and central Pacific receive relatively little aeolian iron.

[14] There is a sink of iron due to the scavenging of dissolved iron onto sinking particles. In addition, free iron, Fe', can be bound with organic ligands, L, to form a complex, FeL, and the complexed form may be less susceptible to scavenging. Field studies show that the majority of "dissolved" iron in the ocean is in the complexed form [*Gledhill and van den Berg*, 1994; *Rue and Bruland*, 1995; *van den Berg*, 1995; *Rue and Bruland*, 1997; *Witter and Luther*, 1998; *Boye et al.*, 2001, 2003]. *Boye et al.* [2003], in fact, find that at least 97% of iron is ligand bound. We represent these processes explicitly as described by *Parekh et al.* [2004, submitted manuscript, 2005], which is closely related to the approach of *Archer and Johnson* [2000]. We carry a total dissolved iron pool, Fe_T, and assume that the complexation reactions are sufficiently rapid [*Rose and Waite*, 2003; *Witter et al.*, 2000] that the partitioning between free iron, Fe', and the complexed form FeL reaches equilibrium quicker than our tracer time step. This equilibrium is described by

$$\beta = \frac{[FeL]}{[Fe'][L']}, \tag{1}$$

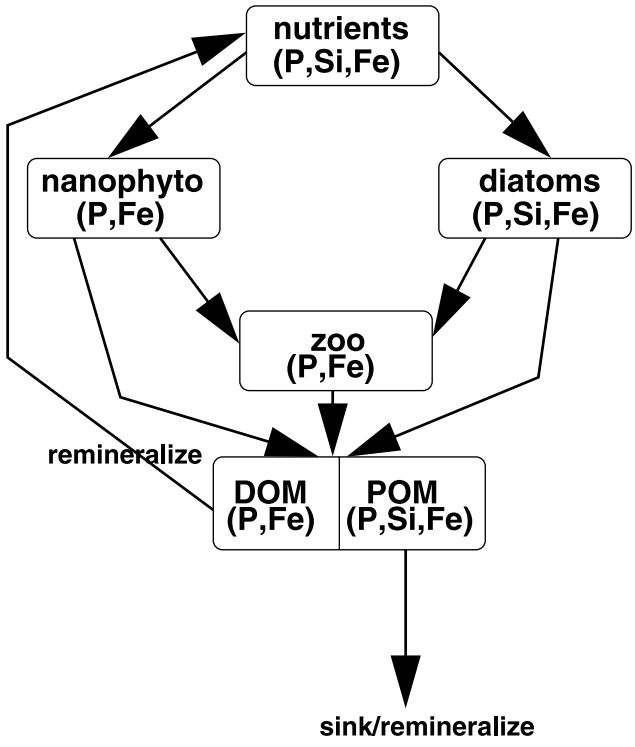

Figure 4. Schematic of ecosystem model, showing flow of the three elements (phosphorus, silicon, and iron) through the nutrient, plankton, and detrital organic matter pools.

where the conditional stability coefficient, β, is specified within the range estimated from laboratory and field studies [*Gledhill and van den Berg*, 1994; *van den Berg*, 1995; *Rue and Bruland*, 1995, 1997]. The total ligand concentration, $L' + FeL$, is uniformly prescribed, here with a value of 1 nM. In the model it is assumed that iron in the complexed form cannot be scavenged. We parameterize scavenging as a first-order process, proportional to the free iron concentration, [Fe']. This parameterization is the same as that of *Parekh et al.* [2004], but differs slightly from that of Parekh et al. (submitted manuscript, 2005) where the scavenging is also a function of particulate matter present. The reasonable range of parameter values was discussed in detail by *Parekh et al.* [2004]. We chose values within ranges suggested by that study and observations (see Appendix A).

[15] While the previously published global ecosystem models of *Aumont et al.* [2003], *Gregg et al.* [2003], and *Moore et al.* [2002b] included a representation of the iron cycle with scavenging and aeolian deposition, none explicitly represented the role of complexation, which modifies the sensitivity of Southern Ocean productivity to changes in the aeolian iron supply, and allows for deepwater interbasin gradients consistent with observations (Parekh et al., submitted manuscript, 2005).

2.3. Ecosystem

[16] We employ an ecosystem model of intermediate complexity, a significantly enhanced version of that used in the Atlantic study of *Dutkiewicz et al.* [2001]. The model has many basic features in common with the recent global models of *Moore et al.* [2002a], *Aumont et al.* [2003], and *Gregg et al.* [2003] and a number of regional model studies [e.g., *Leonard et al.*, 1999; *Chai et al.*, 2002; *Lancelot et al.*, 2000]. We include the potential for colimitation by multiple nutrients (phosphate, iron, silicic acid), light and resolve two functional groups of phytoplankton. Our model is of similar ecological complexity to that of *Aumont et al.* [2003] but simpler than that of *Moore et al.* [2002a] and *Gregg et al.* [2003]. Our aim here was to develop an efficient tool with which to examine the interactions of phosphorus and iron; we include sufficient detail in this model to achieve this goal.

[17] We consider the fate of three chemical elements (phosphorus, silicon, and iron) as they pass from dissolved nutrient forms to phytoplankton, zooplankton, and detritus. The model carries a total of 12 explicit biogeochemical tracers: phosphate PO_4, silicic acid Si, total dissolved inorganic iron Fe_T, phosphorus in small phytoplankton Q_{1_p}, phosphorus in diatoms Q_{2_p}, phosphorus in zooplankton Z_p, iron in zooplankton Z_{fe}, phosphorus in dissolved organic matter DOM_p, iron in dissolved organic matter DOM_{fe}, phosphorus in particulate organic matter POM_p, silicon in particulate organic matter POM_{si}, and iron in particulate organic matter POM_{fe}.

[18] For any tracer, A, the prognostic equation of the model is

$$\frac{\partial A}{\partial t} = -\nabla \cdot \left(\vec{u^*}A\right) + \nabla \cdot (\mathbf{K}\nabla A) + S_A, \tag{2}$$

where $\vec{u}^*$ is the transformed Eulerian mean circulation (which includes Eulerian and eddy-induced advection), **K** is the mixing tensor, and S_A are the sources and sinks due to biological and chemical processes and, in the case of iron, sedimentation and aeolian supply as well. The "SuperBee" second-order flux limiter advection scheme [*Roe*, 1985] is used so as to limit spurious negative in the ecosystem variables. Flux limiter schemes are, however, inherently diffusive; the "SuperBee" is the least diffusive of its class.

[19] Here we briefly describe the biological terms S_A of the ecosystem model that are depicted schematically in Figure 4. Full equations and a further discussion of parameter choices are given in Appendix A. Ecosystem parameters are given in Table 1.

[20] Phytoplankton require nutrients and light in order to grow. Nutrients are supplied to the euphotic zone through ocean transport processes and, in the case of iron, aeolian deposition. Photosynthetically active radiation (PAR) is predicted for each time step as a function of latitude and day of the year following the algorithm of *Paltridge and Platt* [1976]. PAR is attenuated in the water column including a contribution from phytoplankton themselves,

$$I = I_o e^{-(k_w + k_c Chl)z}, \tag{3}$$

where I_o is 24-hour mean PAR incident at surface (W m^{-2}), attenuation coefficients $k_w = 0.04$ m^{-1} for water molecules, and $k_c = 0.05$ m^2 (mg Chl)$^{-1}$ for phytoplankton, Chl (mg m^{-3}) is chlorophyll content of water, and z is depth.

Table 1. Ecosystem Model Parameters[a]

Parameter	Symbol	Value	Units
Phytoplankton growth rates	$\mu_{o_{q1}}$	1/0.8	d^{-1}
	$\mu_{o_{q2}}$	1/0.5	d^{-1}
Zooplankton grazing rate	g_o	1/0.8	d^{-1}
Mortality/excretion rates	m_{q_1}	1/15	d^{-1}
	m_{q_2}	1/15	d^{-1}
	m_z	1/30	d^{-1}
Half saturation constants	$(I)_{q_1}$	30	W m^{-2}
	$(I)_{q_2}$	25	W m^{-2}
	$(PO_4)_{q_1}$	0.05	μM
	$(PO_4)_{q_2}$	0.1	μM
	$(Si)_{q_2}$	2	μM
	$(Fe)_{q_1}$	0.01	nM
	$(Fe)_{q_2}$	0.05	nM
	$(Q)_z$	0.075	μM
Ratios of elements in plankton	$R_{(si:p)_{q2}}$	25	
	$R_{(fe:p)_{q1}}$	1×10^{-4}	
	$R_{(fe:p)_{q2}}$	1×10^{-3}	
Grazing efficiencies	γ_{q_1}	0.3	
	γ_{q_2}	0.3	
Palatability to zooplankton	η_{q_1}	1	
	η_{q_2}	0.4	
Grazing threshold	Q_o	5×10^{-4}	μM
Minimum phytoplankton	Q_e	1×10^{-5}	μM
Minimum zooplankton	Z_e	1×10^{-4}	μM
Partition into DOM/POM	λ_{mq_1}	0.5	
	λ_{mq_2}	0.2	
	λ_{mz}	0.2	
	λ_g	0.5	
Remineralization rates	r_p	1/50	d^{-1}
	r_{si}	1/360	d^{-1}
	r_{fe}	1/50	d^{-1}
Sinking rates	w_p	8	m d^{-1}
	w_{si}	11	m d^{-1}
	w_{fe}	8	m d^{-1}
Iron solubility constant	α	0.025	
Iron scavenging rate	κ_s	1×10^{-3}	d^{-1}
Ligand binding strength	β	1×10^5	$(\mu M)^{-1}$
Max Chl:P ratio	$B^{\max}$	40	mg Chl (mmol P)$^{-1}$
Min Chl:P ratio	$B^{\min}$	16	mg Chl (mmol P)$^{-1}$
Critical irradiance	I_*	90	W m^{-2}

[a]See Appendix A for more details.

Light is assumed not to reach the ocean surface when ice is present. Monthly fractional ice coverage is specified in the model based on observed data, following OCMIP [*Dutay et al.*, 2002].

[21] The explicit representation of silicon in the model facilitates the representation of two "classes," or functional groups, of phytoplankton: diatoms (which need silicic acid) and nano/pico phytoplankton, which we will refer to as "small" plankton, and which do not utilize the silicic acid pool. Similar approaches have been used in other intermediate complexity models [e.g., *Aumont et al.*, 2003]. *Moore et al.* [2002a] additionally represent diazotrophs (and an explicit nitrogen limitation), and *Gregg et al.* [2003] also include chlorophytes, cyanobacteria, and coccolithophores. The growth of the phytoplankton is limited by the least abundant nutrient following a Michaelis-Menton type parameterization (see Appendix A for the growth rates μ_{q_1} and μ_{q_2}). The two classes of phytoplankton are differentiated by their nutrient requirements, nutrient stoichiometry, and growth rates. For simplicity, the ratio of the uptake of silicic acid to phosphate in diatoms ($R_{(si:p)_{q2}}$) is assumed constant in this model. However, in reality this ratio varies with iron and light limitation [*Franck et al.*, 2000]. Changes to this uptake rate probably have important consequences to the Southern Ocean export ratio, and consequently the supply to most of the ocean thermocline [*Sarmiento et al.*, 2004; *Matsumoto et al.*, 2002]. These consequences are not addressed in this study. We impose ratios of iron to phosphate uptake ($R_{(fe:p)_{q1}}$, $R_{(fe:p)_{q2}}$) which differ between phytoplankton classes but which are otherwise treated as constants. Diatoms have a higher iron to phosphorus stoichiometry than do the small phytoplankton [*Sunda et al.*, 1991; *Sunda and Huntsman*, 1995]. The choice to treat these as constant values is, as with $R_{(si:p)_{q2}}$, a simplification. The ratios probably vary with region and between species within our two functional groups [*Sunda*, 1997]. The phytoplankton classes also differ in their palatability to the single explicit grazer, which is parameterized following *Evans* [1988], and grazing rates, g_{q_1} and g_{q_2}, are given in Appendix A. The larger and silica protected diatoms are assumed less palatable. Silicon is modeled as passing immediately through the zooplankton following *Chai et al.* [2002]. The iron content of zooplankton is variable depending on the quantities of each type of phytoplankton that are consumed.

[22] Mortality (and excretion) of phytoplankton and grazers, along with sloppy grazing, supplies organic matter to the two pools: a dissolved (semi-labile) organic pool which is neutrally buoyant in the water column and a particulate pool which sinks gravitationally with assumed constant speed. The division between the two pools (by fraction λ; see Appendix A) is different for each plankton group and different for organic matter formed by mortality and sloppy grazing. Diatoms provide proportionally more material to the particulate pools than small phytoplankton. The rate at which these pools remineralize back to the inorganic pools also differs between elements: Silicon remineralizes more slowly than phosphorus and iron, leading to longer remineralization length scales and an accumulation of silicic acid near the ocean floor [see, e.g., *Gnanadesikan*, 1999; *Tréguer et al.*, 1995]. The elemental composition of the pools reflects the composition and fractional contributions from each of the source organisms. However, there is no dissolved organic silicon pool; detrital silicon is assumed to occur only in the particulate form. Particulate organic matters sinks with a constant rate, with a faster sinking rate for the particulate silicon pool (following *Chai et al.* [2002]).

3. Control Experiment

[23] The full set of biogeochemical prognostic equations is listed in Appendix A, and parameter values used for the control run (and subsequent sensitivity runs) are given in Table 1. Where experimentally determined ranges are known, parameter values are chosen to be consistent. Phosphate and silicic acid distributions are initialized with observed climatologies [*Conkright et al.*, 2002] and total dissolved iron from a previous modeling study (Parekh et al., submitted manuscript, 2005). The ecological variables are initialized with arbitrary, small concentrations, and the full physical-biogeochemical-ecological model is integrated

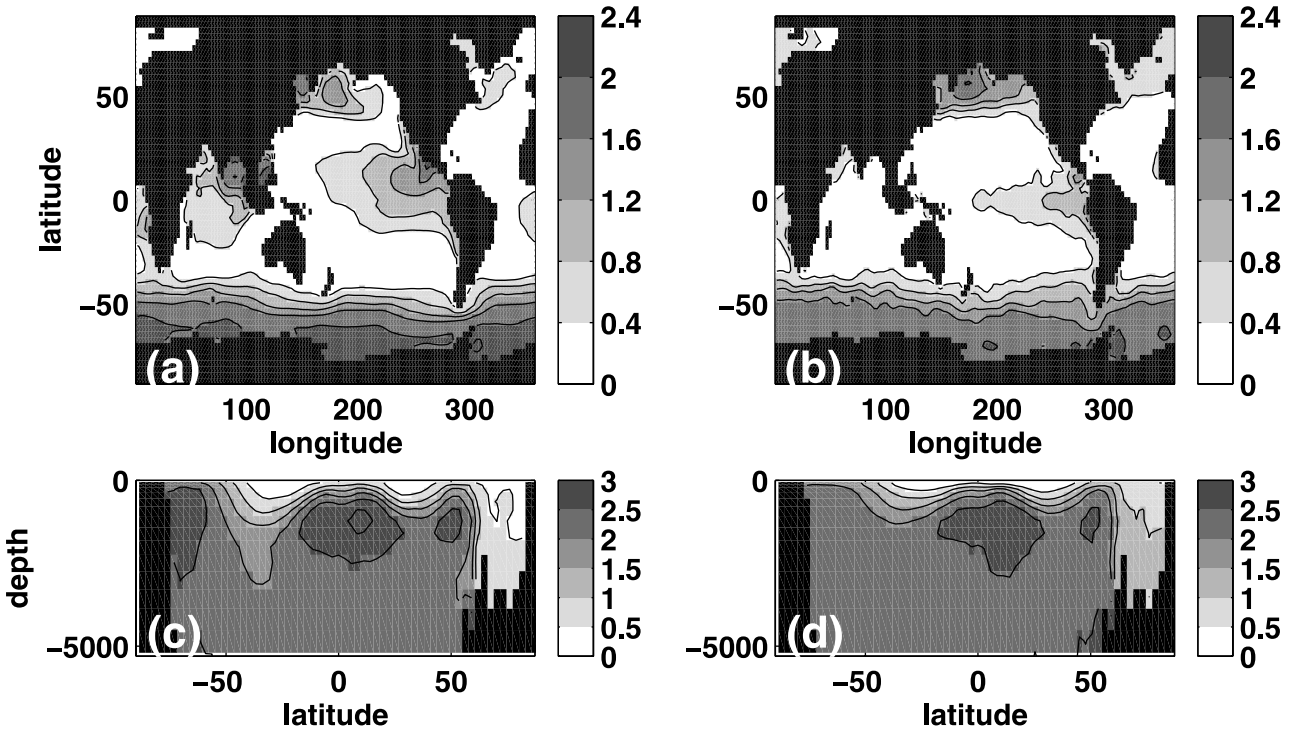

Figure 5. Annual mean PO_4 (μM). (a) Model control run surface. (b) Observed surface. (c) Model control run zonally averaged meridional transect. (d) Observed zonally averaged meridional transect. Observed climatology is from *Conkright et al.* [2002]. Contour intervals are 0.4 μM for surface figures and 0.5 μM for transects.

for 3000 years, approaching a long-term steady state: Global primary production shows no drift and there is a very minimal, continuing adjustment in the nutrient distribution of the oldest waters of the deep Pacific. The control run is forced with monthly mean [*Mahowald et al.*, 2003] dust fluxes (Figure 3). We assume a solubility of this iron of 2.5%, which is within the range (1–10%) suggested by recent studies [*Jickells and Spokes*, 2001; *Duce and Tindale*, 1991], but less than suggested by *Johnson et al.* [2003] and *Gao et al.* [2003].

3.1. Nutrient Distributions

[24] Since the nutrient fields are fully prognostic, and we are particularly interested in the sensitivity of their coupled cycles, we illustrate and discuss the modeled surface distributions and zonally averaged meridional transects of the control run in relation to observed fields.

3.1.1. Phosphate

[25] Figure 5 shows the surface and zonally averaged transects of phosphate for the model ocean and for observations [*Conkright et al.*, 2002]. The qualitative, basin-to-basin patterns are consistent with the observed distributions with elevated surface concentrations in the Southern Ocean, tropical Pacific, and subarctic Pacific. Surface phosphate is generally depleted in the Atlantic, as is observed.

[26] The large oligotrophic regions of the subtropical gyres are reproduced. The meridional transects of phosphate also compare well, picking out the prominent low values in the thermocline of the subtropical gyres and the nutrient-rich upwelling regions. Phosphate is enriched in the subsurface tropical oceans due to nutrient trapping, which is a little overestimated at this coarse resolution [e.g., *Najjar et al.*, 1992; *Aumont et al.*, 1999]. Phosphate is somewhat low in the northern North Atlantic, perhaps due to the lack of flow through the Arctic Ocean, or poor representation of the subantarctic mode waters which probably feed nutrients to the thermocline [*Sarmiento et al.*, 2004]. Southern Hemisphere thermocline water phosphate is too low in the model.

[27] Some regional features in the tropical oceans which are not so consistent with the observations may be attributable to the relatively coarse resolution of the circulation model used here. In particular, phosphate is "trapped" in the Indonesian archipelago where the bathymetry is coarsely resolved. In addition, the low resolution of this configuration does not properly represent the role of the undercurrents in supplying nutrients to the surface of the tropical Pacific [e.g., *Aumont et al.*, 1999]. Consequently, the waters supplying the surface tropical Pacific are from too great a depth: These waters are too rich in phosphate and too iron-depleted. Surface phosphate in parts of this region is therefore higher than in observations. These issues may also be partially attributable to the poorly constrained external iron sources. Riverine and hydrothermal iron sources are not represented here, but may be important, particularly for the Western Central Pacific [e.g., *Christian et al.*, 2002; *Gordon et al.*, 1997]. This, too, might explain

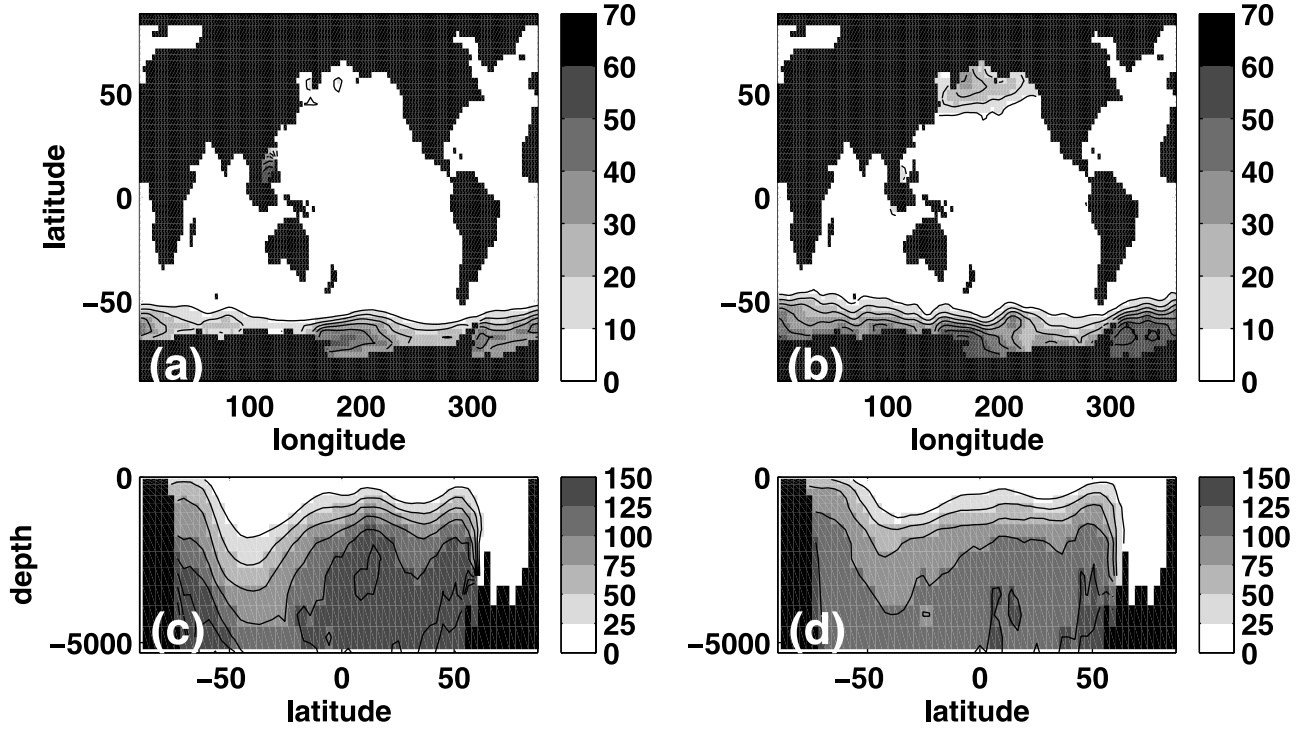

Figure 6. Annual mean surface dissolved inorganic silicic acid (μM). (a) Model control run surface. (b) Observed surface. (c) Model control run zonally averaged meridional transect. (d) Observed zonally averaged meridional transect. Observed data climatology is from *Conkright et al.* [2002]. Contour intervals are 10 μM for surface and 25 μM for transects.

the discrepancy between model and observations in the northern Indian Ocean.

3.1.2. Silicic Acid

[28] Silica (shown in Figure 6) remineralizes deeper in the water column than phosphorus [*Tréguer et al.*, 1995; *Gnanadesikan and Toggweiler*, 1999], which is reflected in the slower remineralization timescale and faster sinking speeds in this model. Because of this, its pathways to the surface ocean are also somewhat different [see *Brzezinski et al.*, 2002; *Sarmiento et al.*, 2004]. In this model the upwelling of deep waters in the Southern Ocean represents the major route by which silicic acid is returned to the surface global ocean (Figure 1b). *Sarmiento et al.* [2004] also hypothesize that preferential stripping of silicic acid in the Southern Ocean leads to mode water that is low in silicic acid. This will also lead to the differences in profiles between silicic acid and phosphate.

[29] The model qualitatively reproduces the broad gyre and basin scale patterns and gradients of silicic acid in the oceans. For the given circulation and parameters, we do find a slight overestimation of the deep Pacific silicic acid concentration, and slightly low values are found too deep in thermocline and surface waters; this is particularly noticeable in the subarctic North Pacific. In this latter region, the coarse configuration of the model probably does not capture the formation of the intermediate waters correctly, and thus underestimates the nutrients in the surface. This is a common problem in numerical models [*Gnanadesikan et al.*, 2002]. *Sarmiento et al.* [2004] additionally suggest that tidal mixing in the North Pacific may be an important supply of nutrients to the surface waters, a process not explicitly represented in the model. Similar to phosphate, silicic acid in the northern North Atlantic is too low (around 1 μM while observations are around 5 μM). This discrepancy could be due to the lack of flow through the Arctic Ocean, as well as poor representation of the subantarctic mode waters.

3.1.3. Dissolved Iron

[30] The modeled total dissolved iron distribution, shown in Figure 7, captures the broad basin to basin gradients implied from the, as yet sparse, observations (compiled by Parekh et al. (submitted manuscript, 2005) and *Gregg et al.* [2003]). Modeled surface iron concentrations are high under the dust plumes in the North Atlantic and in the Indian Ocean and low in the remote Pacific and Southern oceans. Deep values are slightly higher in the Pacific and Southern oceans than they were at the surface (also consistent with observations (Parekh et al., submitted manuscript, 2005)). The modeled iron distribution, and the mechanisms controlling it, are largely consistent with the previous models of *Parekh et al.* [2004, submitted manuscript, 2005].

[31] Over much of the ocean, and particularly in the HNLC regions, most of the iron available for photosynthesis is supplied by upwelling and mixing to the surface (as noted by *Fung et al.* [2000], *Aumont et al.* [2003], *Moore et al.* [2002b], and Parekh et al. (submitted manuscript, 2005)). Owing to the decoupling of phosphorus and iron in the deep waters, caused by the additional processes of

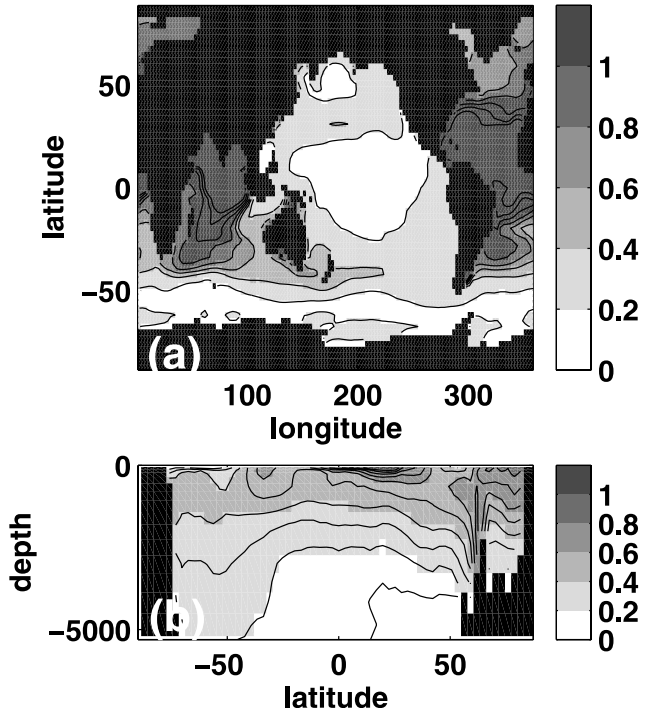

Figure 7. Model control run annual mean iron (nM). (a) Surface and (b) zonally averaged meridional transect. Observations are sparse; see Parekh et al. (submitted manuscript, 2005) for representation of observed data. Contour interval is 0.2 nM for both panels.

scavenging and complexation which affect iron, the waters supplied to the surface are deficient in iron (with regards to the consumption of phosphate in primary production) over most of the globe. This deficit is most significant in regions where older, deeper waters are upwelled to the surface: the subpolar and tropical regions. In other regions of the ocean, the aeolian iron supply is sufficient to overcome this deficit, but not in the so-called HNLC regions, where primary production is iron limited. In Figure 8, shaded areas depict the regions where iron is the limiting nutrient for (Figure 8a) small phytoplankton and (Figure 8b) diatoms. Here we use the annual average concentration for each of the nutrients and determine where the iron is most limiting relative to its half-saturation value. These areas are, notably, the classic HNLC regimes of the Southern Ocean, Tropical Pacific, and subarctic Pacific. Throughout the Atlantic basin the aeolian supply is strong enough that iron is not limiting. We believe the region of iron limitation near to Indonesia is an artifact of the model due to the omission of riverine sources [*Gordon et al.*, 1997; *Mackey et al.*, 2002]. Although the diatom class has a higher iron requirement than small phytoplankton, the regions where it is predominantly iron limited are generally smaller; silicic acid limitation becomes more significant than iron in many regions.

3.2. Chlorophyll and Primary Productivity

[32] Modeled chlorophyll fields are qualitatively consistent with observations (Figure 9), picking out the major observed regimes. There is a strong standing stock in the upwelling regions, even where they are iron limited (see above), and the model reproduces the characteristic low chlorophyll signature of the oligotrophic subtropical gyres. The modeled Southern Ocean chlorophyll levels are generally a little higher than that inferred from remote ocean color observations in the Southern Ocean. This may be due to unrealistic trapping of nutrients subsurface, but it has also been suggested that, owing to subsurface productivity, the estimates based on remote observations may be biased on the low side [*Schlitzer*, 2002]. Model diagnostics here are, by construction, evaluated over the upper 50 m of the water column, while the analysis of remote observations reflects chlorophyll observed in the first optical depth, which may

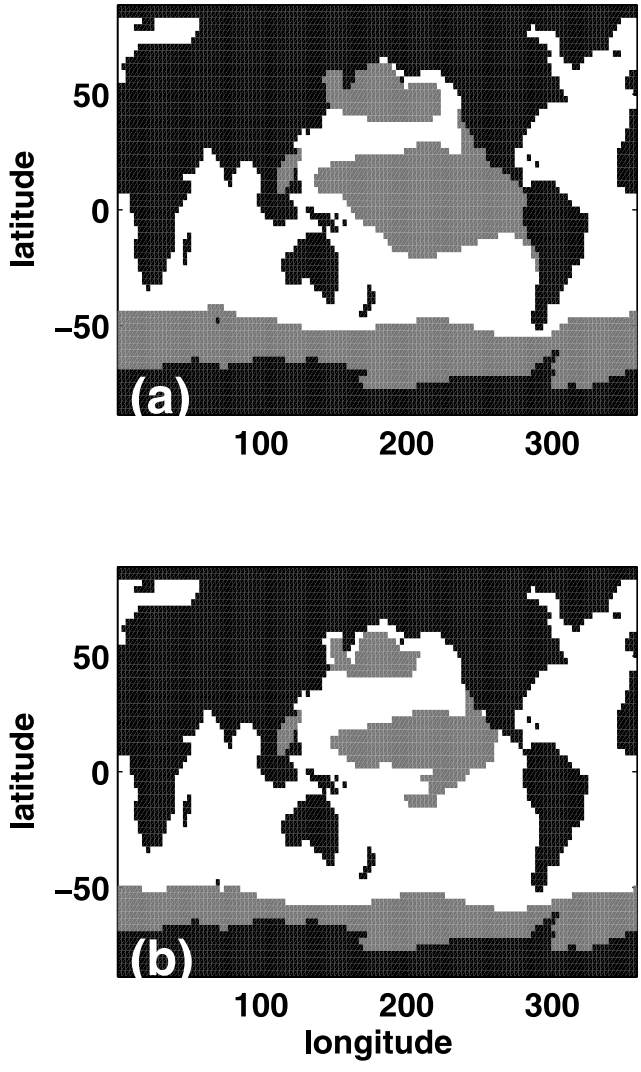

Figure 8. Iron limitation. Shaded regions indicate where iron is limiting nutrient for (a) small phytoplankton and (b) diatoms. Area shaded indicates where $\frac{Fe_T}{Fe_T+(Fe)_{q_1}} < \frac{PO_4}{PO_4+(PO_4)_{q_1}}$ for Figure 8a and $\frac{Fe_T}{Fe_T+(Fe)_{q_2}} < \frac{PO_4}{PO_4+(PO_4)_{q_2}}$ and $\frac{Fe_T}{Fe_T+(Fe)_{q_2}} < \frac{Si}{Si+(Si)_{q_2}}$ for Figure 8b. Annual mean nutrient concentrations are used in this calculation.

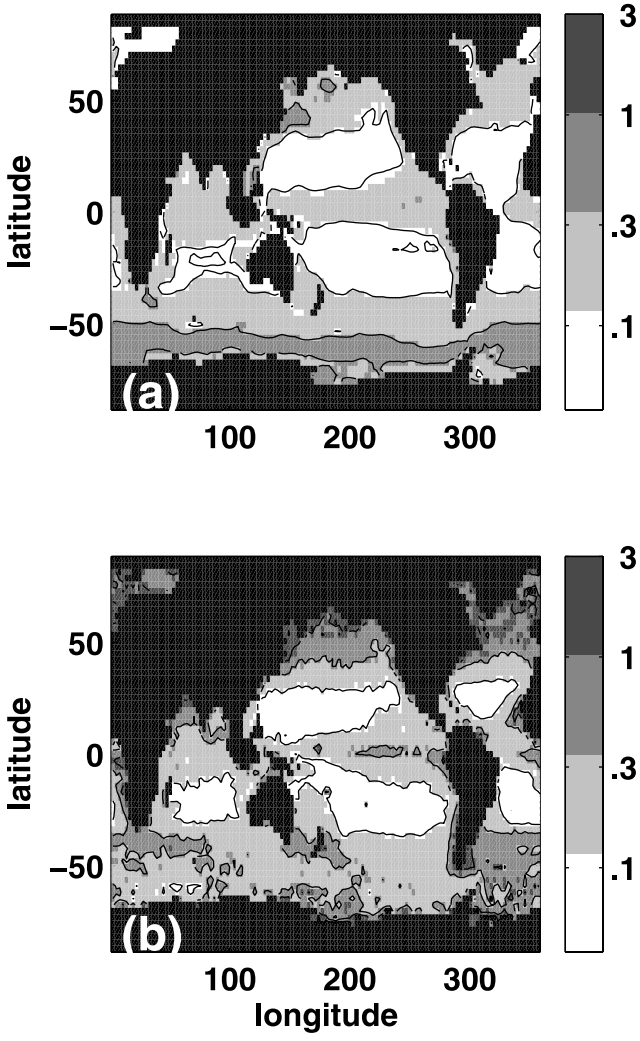

Figure 9. Annual mean surface chlorophyll (mg m^{-3}). (a) Model control run and (b) derivation from SeaWiFS data. Shading is based on a log scale; contours are at 0.1, 0.3, 1, and 3 mg m^{-3}.

be considerably shallower in regions of high productivity. In addition, the modeled fields are smoother, reflecting in part the coarse resolution. The modeled North Atlantic bloom is not as vigorous as observed, particularly in the subpolar gyre, due to the modeled phosphate and silicic acid concentrations being lower than observations in this basin (discussed in sections 3.1.1 and 3.1.2). This does lead, unrealistically, to regions of the North Pacific where the spring bloom is higher than in the North Atlantic.

[33] Globally, diatoms account for 30% of the phosphorus in modeled phytoplankton biomass, consistent with the models of *Aumont et al.* [2003] and *Moore et al.* [2002b]. Owing to the silicic acid requirement of the diatom class, it dominates the ecosystem south of 50°S. To the north of the Antarctic Circumpolar Current, small phytoplankton dominate (consistent with observations [*de Baar et al.*, 1999]). The modeled equatorial Pacific is richer in diatoms than observations suggest [*Gregg et al.*, 2003], consistent with the upwelling of waters from too great a depth to the surface of this region (as discussed above). In contrast, we find too few diatoms in our modeled North Atlantic where silicic acid concentrations are too low. Small phytoplankton dominate in the low nutrient subtropical gyres, resulting in more efficient recycling and a smaller export ratio, and consistent with observations [*Eppley and Peterson*, 1979].

[34] Total global primary production in the control run is 35 GtC yr^{-1} which, given the large uncertainties, is consistent with the range suggested by observational compilations and interpretations of remote ocean color observations (36–57 GtC yr^{-1} [*Longhurst et al.*, 1995; *Antoine et al.*, 1996; *Behrenfeld and Falkowski*, 1997]). The coarse resolution of the model would lead us to expect a low end estimate of global production since the productive coastal margins and eddy-pumping mechanisms, significant in the open ocean [e.g., *Falkowski et al.*, 1991; *McGillicuddy and Robinson*, 1997], are not explicitly resolved. The total global export production through 120 m is 15 GtC yr^{-1}. This is also within the range suggested by inverse models and studies based on remote estimates (10 GtC yr^{-1} [*Usbeck et al.*, 2003]; 11 to 21 GtC yr^{-1} [*Laws et al.*, 2000]). However, relative to the model's primary production, this number is high, indicating that the modeled export is perhaps a little too efficient.

[35] In summary, the physical-biogeochemical-ecological model described above qualitatively captures the broad gyre and basin scale patterns of circulation, productivity, and nutrient distributions in the ocean today. The interplay of parameterized nutrient cycles and ecosystem leads to an explicit emergence of iron limited, upwelling, HNLC regimes and downwelling, macro-nutrient limited, subtropical gyres in the model. The model has some limitations, of course, but remains a useful tool to explore the mechanistic interactions of such a complex system in a qualitative manner. Of particular interest in this model is the interplay of the ecosystem, iron, and phosphorus cycles and the resulting control on regional and global productivity.

4. Sensitivity to Idealized Aeolian Dust Fluxes

[36] It has become clear that iron, through the regulation of productivity, has a significant control on other global biogeochemical cycles, including that of carbon [*Martin*, 1990; *Petit et al.*, 1999]. However, until recently, ocean models have not explicitly represented the oceanic iron cycle, and recent ecosystem models have typically not explicitly included the effects of complexation [*Moore et al.*, 2002a; *Aumont et al.*, 2003; *Gregg et al.*, 2003], though this important process has significant implications for the sensitivity of the system [*Parekh et al.*, 2004].

[37] Here we have coupled a dynamic representation of the oceanic iron cycle to the cycles of other nutrients and an explicit ecosystem. In a suite of idealized, sensitivity experiments we use the model to examine the sensitivity of patterns and rates of oceanic productivity in the model system to variations in the pattern and magnitude of the aeolian iron supply to the surface ocean. While this study is somewhat idealized, it is designed to help understand the interactions by which ocean productivity (and, by inference, the biological pump of carbon) may be linked to, and

Table 2. Results of Experiments[a]

Experiment Name	Fe Flux, mmol m^{-2} yr^{-1}	PP, GtC yr^{-1}	EP, GtC yr^{-1}	Low PO_4 Area, million km^2	Low PP Area, million km^2
Control	variable	34.794	14.334	122	80
Unnamed[b]	6	36.734	14.987	151	101
High	3	36.716	14.981	151	100
Unnamed[b]	0.6	36.234	14.813	147	96
Medium	0.3	35.498	14.607	142	91
Unnamed[b]	0.25	33.671	14.004	118	75
Low	0.15	26.379	11.150	34	65
Unnamed[b]	0.03	15.070	5.853	0	266

[a]First row is the control run using monthly *Mahowald et al.* [2003] dust fluxes. "PP" denotes annual mean primary production, and "EP" denotes annual mean export though 120 m. We denote "low PO_4 area" as $PO_4 < 0.2$ μM and "low PP area" as annual mean primary production <50 gC m^{-2} yr^{-1}. The global mean value of the iron flux in the control run is 0.75 mmol m^{-2} yr^{-1}.

[b]These experiments were not assigned names.

controlled by, the delivery of iron via the atmosphere to the oceans. It is of significance for our understanding of past climates, future changes, and the consequences of artificially supplying the ocean with iron.

[38] In a linked set of seven idealized sensitivity experiments, we remove all regional variation in aeolian iron supply and apply uniform dust fluxes across the entire ocean. The magnitude of this uniform dust flux is modulated (see Table 2) from a very low flux of iron (0.03 mmol Fe m^{-2} yr^{-1}), typical of the present-day remote Southern Hemisphere, to uniformly strong fluxes comparable to that to the present North Atlantic and Indian Ocean (6 mmol Fe m^{-2} yr^{-1}). Initializing each experiment with the fully spun up "control" system described in section 3, we change prescribed aeolian iron supply and integrate the model for several hundred years further, approaching a new, modified steady state. Much of the present ocean experiences an aeolian iron supply of less than 0.3 mmol Fe m^{-2} yr^{-1} (see shading in Figure 3), and only a few regions receive as much as 3 mmol Fe m^{-2} yr^{-1}. Hence, for clarity, we focus on the results from three of the sensitivity tests with "low" (0.15 mmol Fe m^{-2} yr^{-1}), "medium" (0.3 mmol Fe m^{-2} yr^{-1}), and "high" (3 mmol Fe m^{-2} yr^{-1}) uniform aeolian iron fluxes.

[39] These experiments with spatially uniform aeolian iron supply are, of course, highly idealized. Modulating the amplitude of the *Mahowald et al.* [2003] dust flux pattern leads to qualitatively similar results (not shown here). However, the idealized studies provide a clean and clear insight into the large-scale nutrient cycle interactions.

4.1. Global Results

[40] Figure 10 shows time series of total global primary production in the three sensitivity experiments. While primary production rates have approached steady state in the high and medium aeolian flux cases, there is still a small drift in the low dust case. In these idealized sensitivity studies, a global increase in the dust flux to the surface ocean increases global primary productivity. There is an asymmetry in the response to decreasing and increasing the aeolian iron supply, with a decrease in dust leading to a significantly stronger global response in both primary and export productivity (Table 2).

[41] A tenfold increase in aeolian iron supply has resulted in an increase of less than 10% in global productivity. Previous models [*Archer et al.*, 2000; *Watson et al.*, 2000; *Bopp et al.*, 2003] have also shown relatively modest responses in global productivity and, particularly, the enhancement of the biological pump and reduction of atmospheric pCO_2, when the aeolian iron supply is increased to the levels thought to have occurred at the Last Glacial Maximum [*Mahowald et al.*, 1999]. Here we attribute this to several mechanisms: First, as the aeolian dust flux increases, the organic ligand becomes saturated and excess iron, in free form, becomes scavenged. Deep iron concentrations, even in the "high" dust, case remain below 1 nM,

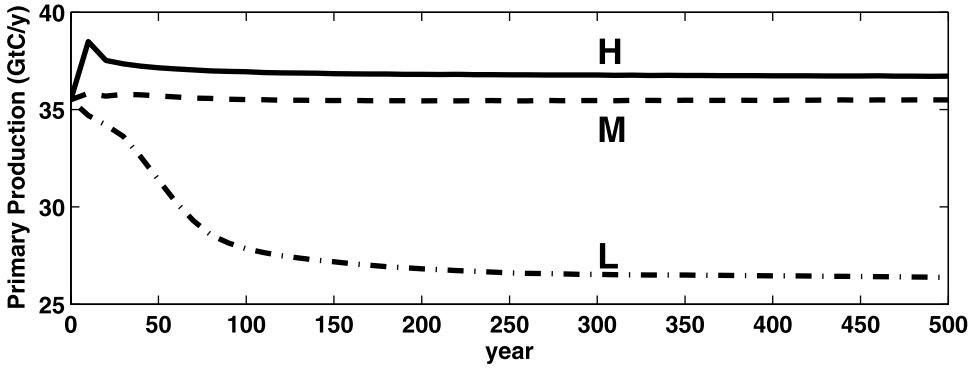

Figure 10. Time series of total global primary production (GtC yr^{-1}) for high (solid line), medium (dashed line), and low (dash-dotted line) dust sensitivity studies.

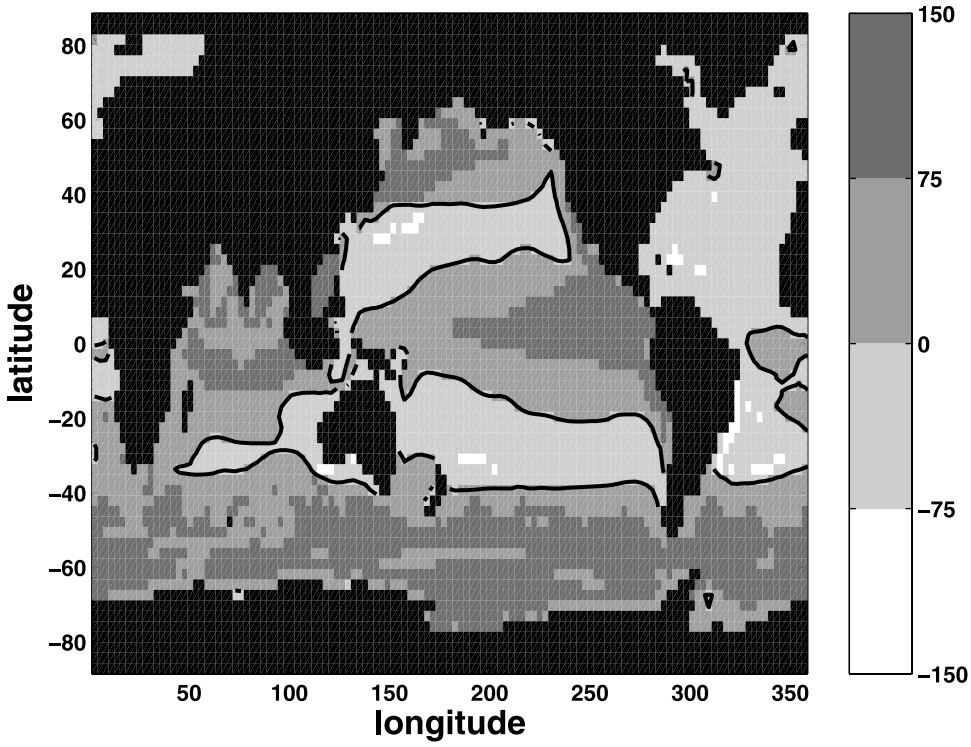

Figure 11. Difference in primary production (gC m^{-2} yr^{-1}) between high and low dust sensitivity studies. Solid line is zero contour. Positive values indicate higher production when aeolian dust supply is enhanced. See color version of this figure at back of this issue.

the prescribed total ligand concentration. (In the real ocean there is a potential that the ligand concentration increases with increased productivity. However, very little is know about the ligand, and here we assume a uniform constant ligand concentration.) Second, even in iron replete surface waters, there are other factors which can limit phytoplankton growth: macro-nutrients, light, grazing. Third, as discussed below, some regions respond with decreased productivity with increased dust flux. These three factors contribute to the model's quick asymptote to a maximum global productivity with increasing aeolian iron supply (see Table 2).

[42] As the global mean aeolian deposition of iron is decreased (by only a factor 2; see Figure 10), there is a very strong response in productivity and continued adjustment after several hundred years with a decrease in global primary production of about 25%. In this case, the deep ocean total dissolved iron concentration and transport to the surface Southern Ocean are significantly decreased. The surface ocean in the upwelling regions rapidly becomes more iron stressed, and the iron limited regions increase significantly in areal extent. In such a scenario, the role of riverine and hydrothermal sources (not represented here) may be significantly enhanced.

[43] Hence the sensitivity studies suggest an asymmetric response to changes in the global aeolian iron supply. Consistent with prior modeling studies, the response to increasing iron supply is limited but the impact of relatively small reductions in aeolian supply is, perhaps surprisingly, strong. While we must regard these findings cautiously, owing to uncertainties in the iron model (for instance the prescribed uniform total ligand concentration), this is an important and significant implication which we should consider. Most such studies to date have focused on the increased dust flux scenario because of its relevance to glacial conditions and the drawdown of atmospheric pCO_2 in cooler, drier climates. However, we suggest that there might be much more significant consequences for ocean productivity and the biological carbon pumps in a warmer, wetter climate where aeolian iron supply may be suppressed. Such conditions are thought to have occurred in warm, past climates such as the late Permian [e.g., *Kutzbach and Gallimore*, 1989] and could be a consequence of future shifts to a warmer climate state [e.g., *Covey et al.*, 2003]. Our model suggests a positive feedback with warmer, wetter climate suppressing the aeolian iron supply, reducing the effectiveness of the ocean's biological carbon pumps and increasing atmospheric CO_2.

4.2. Regional Responses

[44] The response to modulation of the aeolian iron flux is not uniform. The variation of regional response in these sensitivity studies reveals the interplay of iron and phosphorus cycles, and pathways of nutrient supply to the surface ocean in this global model. We illustrate the variable regional response in Figure 11, which shows the difference in primary production between the "high" and "low" dust cases. The figure may be summarized as follows: With increased aeolian iron supply, primary production (1) increases in the upwelling regions of the Southern Ocean

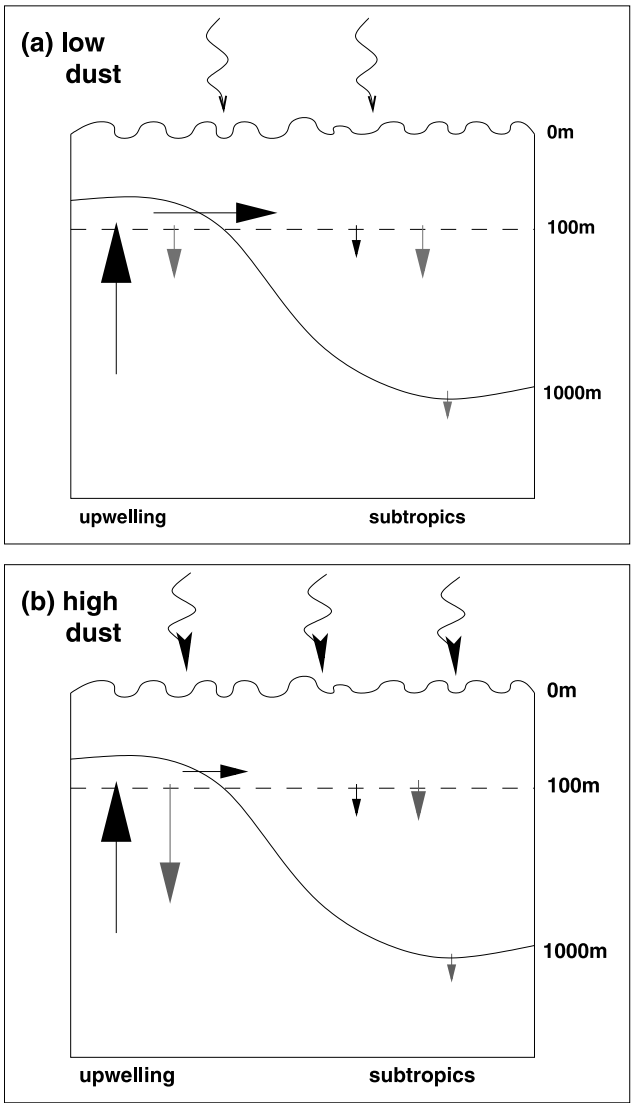

Figure 12. Schematic of supply of macro-nutrients and export of organic matter in (a) low and (b) high dust experiments. Curved line indicates isopycnal at the base of the thermocline, indicating upwelling and subtropical regions. Wavy arrows represents aeolian dust deposition, black arrows indicate pathway of macro-nutrients, and shaded arrows indicate vertical export of organic matter. Arrow length/width roughly indicates relative magnitudes. In low dust case, productivity in upwelling region is iron limited, and excess macro-nutrients are transported in the Ekman flow to the subtropical gyre. In the high dust case, upwelling macro-nutrients are utilized locally, reducing nutrient supply to the gyre.

and the Indo-Pacific, (2) decreases in the downwelling subtropical gyres of the Indo-Pacific, and (3) decreases throughout the Atlantic basin.

4.2.1. Upwelling Regions of the Southern and Indo-Pacific Oceans

[45] The so-called "High Nitrogen, Low Chlorophyll" (HNLC) regions are all associated with upwelling regimes: the Southern Ocean, Tropical Pacific, and the sub-Arctic Pacific. These regimes are characterized by elevated surface macro-nutrients, and a key question has been what limits the ecosystem from simply consuming those nutrients. It seems that iron limitation is a significant factor [*Martin et al.*, 1987] as witnessed by in situ fertilization experiments [*Martin et al.*, 1994; *Coale et al.*, 1996; *Boyd et al.*, 2000] and supported by recent numerical models [*Archer and Johnson*, 2000; *Fung et al.*, 2000; *Moore et al.*, 2002b; Parekh et al., submitted manuscript, 2005].

[46] This model also supports this notion (see Figure 8), and in our sensitivity experiments, increased aeolian iron supply simply leads to a relief of iron limitation and increased productivity in the HNLC regimes (Figure 11). However, especially in the Southern Ocean, not all macro-nutrients are drawn down. Even with excess iron in the "high" dust experiment, not all macro-nutrients are utilized. This is due to light limitation, as suggested by *Popova et al.* [2000]. In the equatorial Pacific, high zooplankton standing stocks help maintain a limit on phytoplankton biomass in this model. Here, too, even with excess iron, not all macro-nutrients are consumed.

4.2.2. Indo-Pacific Subtropical Gyres

[47] In the Indo-Pacific basin of this model, the subtropical gyres show a decrease in productivity associated with a globally increased aeolian iron supply, in stark contrast with direct response in the upwelling, HNLC regions. This reveals the coupling of the phosphorus and iron cycles, and the coupling of biogeochemical cycles between upwelling and downwelling regimes through the exchange of macro-nutrients.

[48] The question of what sustains the supply of macro-nutrients to the surface of the oligotrophic subtropical gyres has been the topic of many studies. Vertical wintertime convection, "eddy pumping" [*Falkowski et al.*, 1991; *McGillicuddy and Robinson*, 1997; *Oschlies and Garçon*, 1998], smaller, frontal scale features [*Mahadevan and Archer*, 2000; *Lévy et al.*, 2001], induction when the western boundary current interacts with the winter mixed layer [*Williams and Follows*, 2003], and enhanced diapycnal mixing in the western boundary current [*Jenkins and Doney*, 2003] all bring nutrients to the surface subtropics. However, these mechanisms rearrange nutrients within the bowl of the gyre. There is a continual loss of macro-nutrients from the bowl of the subtropical gyre due to the sinking flux of organic material through the base of the thermocline. What balances these losses?

[49] Lateral transport in the Ekman layer [*Williams and Follows*, 1998] and lateral eddy transfers of inorganic and organic nutrients within the euphotic layer [*Oschlies*, 2002; *Lee et al.*, 1997] can play a significant role in maintaining the nutrient loading and productivity of the subtropical gyres. While these sources of nutrients are relatively small compared to new production in the surface of the gyre, they are significant in that they balance the long-term leakage of nutrients across the base of the subtropical thermocline as sinking particles.

[50] While we typically discuss the oligotrophic subtropical gyres and the (HNLC) upwelling regimes in isolation, we see here that they are intimately coupled. We argue that

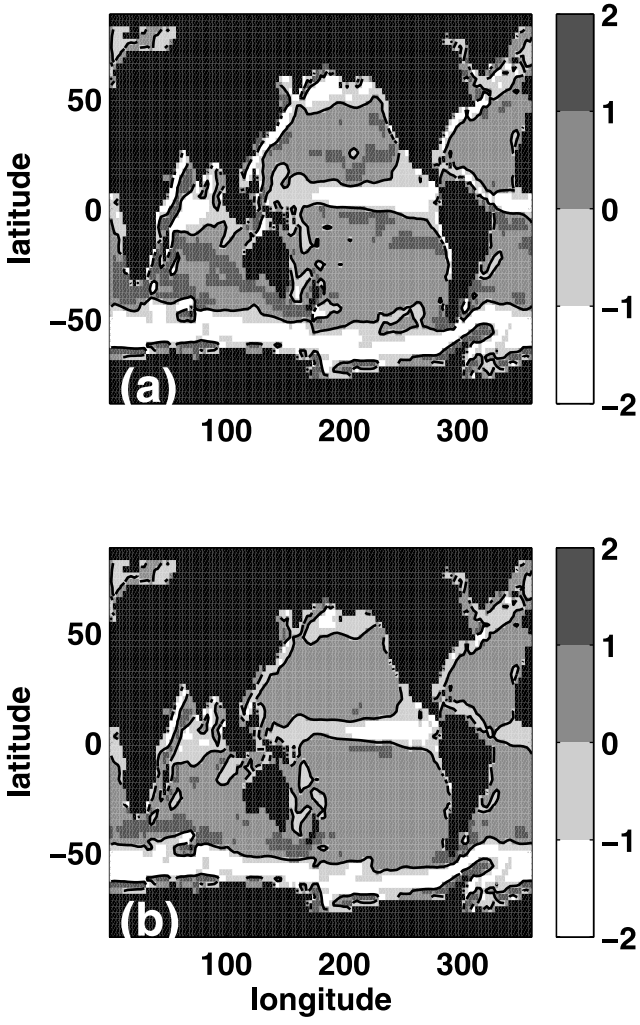

Figure 13. Tendency of phosphate in top layer (0–50 m) of model (μM yr^{-1}) owing to horizontal transport for (a) low and (b) high dust experiments. Negative tendency indicates a net lateral removal of phosphate, and positive indicates a net lateral convergence of phosphate. The advection in this layer is dominated by Ekman dynamics. See color version of this figure at back of this issue.

the long-term maintenance of the integrated macro-nutrient load of the bowl of the subtropical gyre is maintained, in part, by a significant contribution from the lateral Ekman supply bringing nutrients from the enriched surface waters of the subpolar gyre and tropics into the subtropical gyre. This "trickle" of nutrients offsets the sinking particle flux across the base of the thermocline.

[51] Our sensitivity experiments indicate that the degree of iron limitation of the upwelling regions significantly controls the macro-nutrient supply to the subtropics. When the upwelling region is significantly iron limited, surface macro-nutrients are elevated there, and the Ekman supply to the neighboring subtropics is high (Figure 12a). Conversely, the relief of iron limitation in the upwelling region will aggravate the phosphorus limitation of the neighboring subtropics (Figure 12b). In Figure 13 we show the tendency of phosphate due to horizontal advection in the surface level of the model (0–50 m). Ekman advection provides a substantial fraction of the lateral advective transfer in this layer (see model diagnostics of *Williams and Follows* [1998]). Negative values correspond to a lateral advective loss of nutrients from the grid cell, typical of upwelling regions. Positive values show a lateral convergence of nutrients. In the low dust experiment this lateral Ekman convergence in the subtropics is much higher than in the high dust experiment.

[52] We can summarize the results for low dust: (1) There is lower productivity in upwelling regions, (2) Ekman lateral supply of macro-nutrients to neighboring gyres is enhanced, and (3) macro-nutrient limited subtropical gyres respond with increased productivity. Similarly, for high dust, the results are as follows: (1) There is higher productivity in upwelling regions, (2) Ekman lateral supply of macro-nutrients to neighboring gyres is decreased, and (3) macro-nutrient become even more sparse in subtropical gyres and productivity decreases.

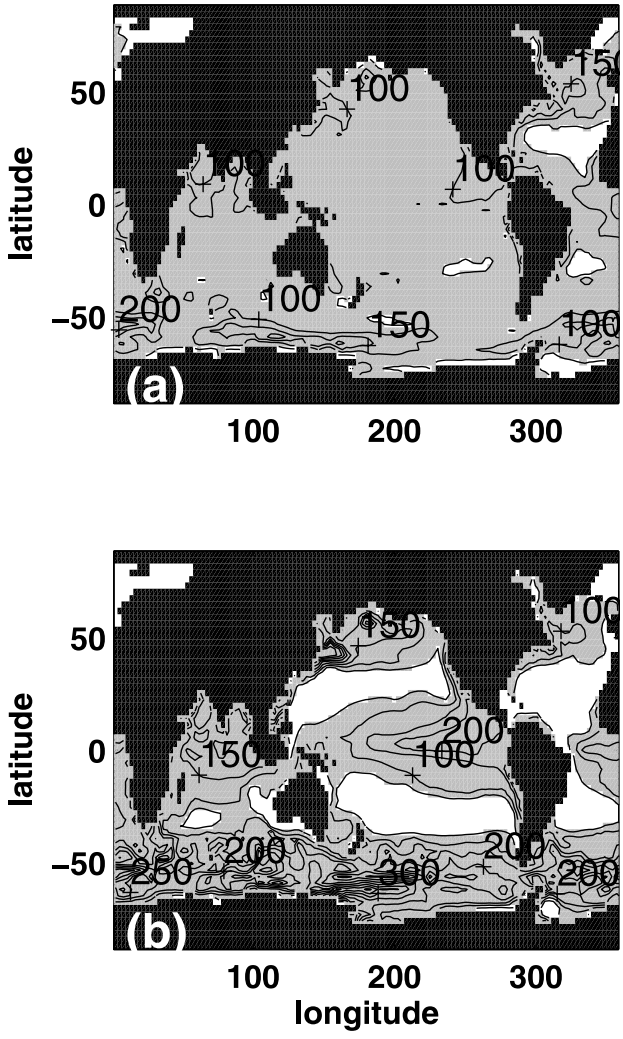

Figure 14. Primary production (gC m^{-2} yr^{-1}) for (a) low and (b) high dust experiments. Contour interval is 50 gC m^{-2} yr^{-1}. Shading indicates production greater than 50 gC m^{-2} yr^{-1}.

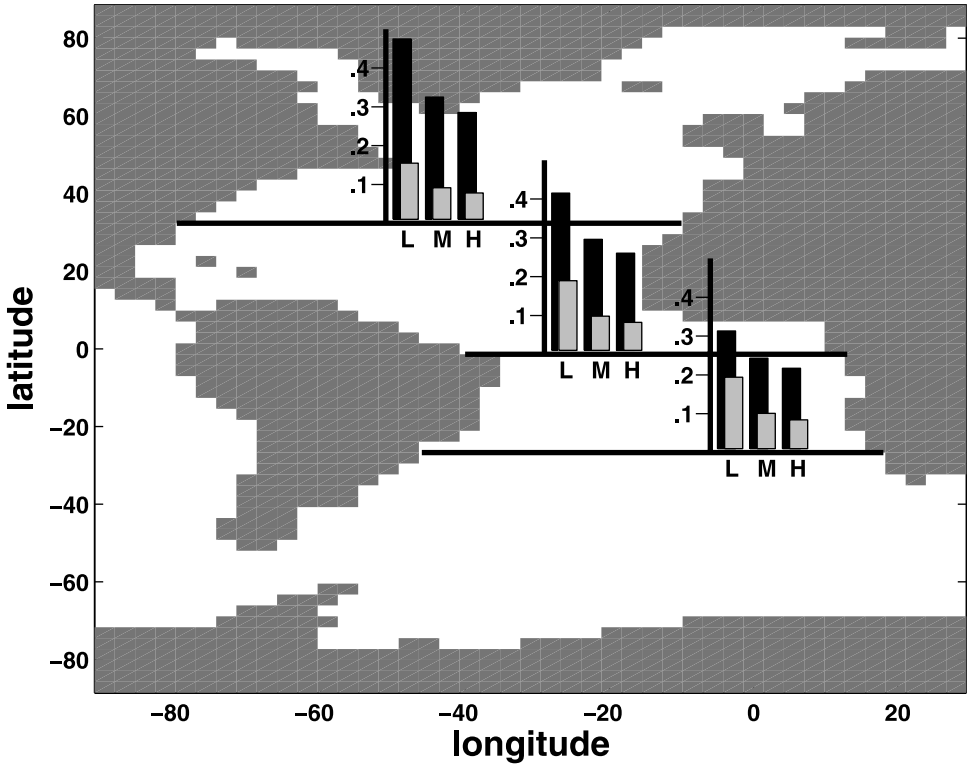

Figure 15. Modeled phosphate transported northward across latitude bands in Atlantic (Tmol P yr^{-1}) for low (L), medium (M), and high (H) dust experiment. Dark bars indicate total nutrients transported across in the 220–1080 m depth, and lighter bars indicate total nutrients transported across in the 0–220 m depth.

[53] We infer from these experiments that surface oriented, lateral Ekman (and perhaps eddy) transfers of macronutrients from the surrounding upwelling regions play a major role in sustaining the integrated nutrient loading of the gyres. The vigor of these lateral supplies is a function of the concentration of nutrients in the surface of the upwelling regions [*Williams and Follows*, 1998; *Williams et al.*, 2000] which may be regulated by the aeolian iron supply (or other changes).

[54] One consequence of these results is that the size of the oligotrophic gyre (defined as low nutrient, low productivity) increases along with aeolian iron supply (see Table 2). Figure 14 shows primary production for the low and high dust experiments. Although the total global production is greater for the high dust experiment, it is constrained to the upwelling regions with large low productivity, low nutrient oligotrophic regions (rather like today's ocean). In the low dust case, we find a more homogeneous ocean, with relatively abundant surface phosphate and moderate production over most of the globe. Iron is the limiting nutrient almost universally, and there is a much weaker distinction between the subtropical and upwelling regimes.

4.2.3. Atlantic Ocean

[55] In contrast to the Southern and Indo-Pacific Oceans, the Atlantic basin in this model responds with uniform sign to changes in the external iron supply. An increase of the aeolian iron flux leads to a decrease in Atlantic productivity, both in the subtropical gyres and in the subpolar North and tropical Atlantic (Figure 11). While there is a significant difference in the aeolian iron deposition between the modern Atlantic and Pacific basins, this is not the case in these sensitivity studies, where the aeolian supply is globally uniform. The Atlantic-Pacific contrast in these sensitivity experiments reflects instead the difference in the Atlantic and Pacific circulation, namely that deep water forms in the North Atlantic, but not in the Pacific. This, in turn, requires that their nutrient budgets are maintained differently.

[56] Strong buoyancy losses in the Norwegian and Labrador Seas drives the formation of North Atlantic Deep Water which flows southward at depth to join the Antarctic circumpolar flow and the global ocean. Surface productivity leads to an export of nutrients from the surface to depths; thus North Atlantic Deep Water accumulates nutrients and removes them from the basin. In order to maintain the nutrient budget on long timescales, these nutrients must be resupplied by mixed layer, mode and thermocline waters entering the basin. *Sarmiento et al.* [2004], using the contrasting patterns of silicic acid and nitrate, highlight the key role of subantarctic mode waters in supplying nutrients to the upper ocean around the globe, including the Atlantic basin. Our model supports this view; there is a northward transport of nutrients into the Atlantic basin in the thermocline.

[57] Figure 15 shows the total northward transport of phosphate across three latitude bands in the North Atlantic

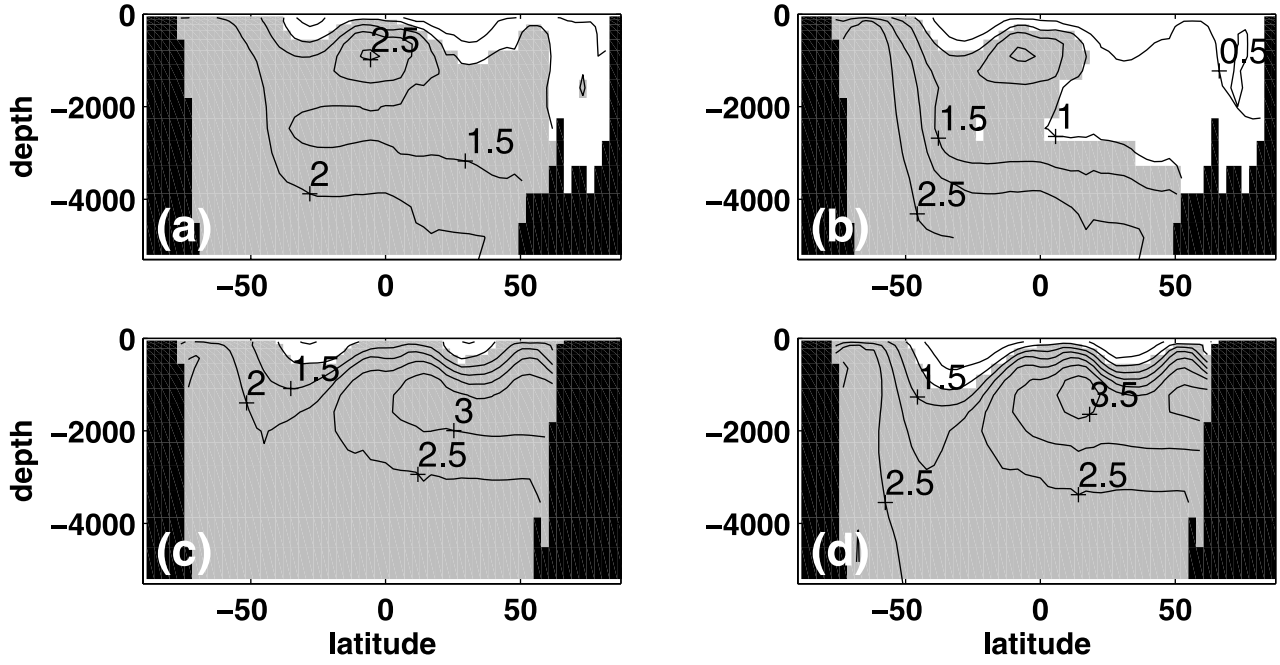

Figure 16. Zonally averaged meridional transects of phosphate (μM) in Atlantic for (a) low and (b) high dust experiments, and in Indo-Pacific for (c) low and (d) high dust experiments. Contour intervals are 0.5 μM. For Figures 16a and 16b, shading indicates values greater than 1 μM; for Figures 16c and 16d, shading indicates values greater than 2.5 μM.

in the seasonal mixed layer water (0 to 220 m) and the thermocline water (220 to 1080 m) for each of the "low," "medium," and "high" dust sensitivity studies. There is significant northward nutrient transport in the thermocline, in part associated with the nutrient streams of the western boundary currents [*Pelegri and Csanady*, 1991]. We also note that there is a smaller, but significant, northward nutrient transport in the upper ocean (0–220 m). This water includes both Ekman transport and water within the seasonal mixed layer. As these waters travel north, nutrients are exported biotically from the upper ocean and accumulate in the thermocline.

[58] In the "high" dust case, there is a significantly decreased advection of phosphorus into the basin in both seasonal mixed layer and thermocline, leading to a reduced Atlantic basin budget. The whole basin becomes more macro-nutrient depleted, and productivity decreases. In the "low" dust case, there is enhanced supply of nutrients into the basin, with the most notable change in the upper (0–220 m) layer. Macro-nutrients accumulate within the basin and productivity increases. This strong enhancement of the upper ocean phosphate flux into the Atlantic occurs in association with waters entering the basin around the tip of Africa (Figure 13).

[59] Figure 16, showing zonally averaged meridional transects of phosphate in the Atlantic and Indo-Pacific basins for the low and high dust cases, illustrates the possibility of a global shift in phosphorus distributions associated with changes in the iron stress. In the low dust case, the macro-nutrient supply to the Atlantic is strong and the mean concentrations are higher, relieving the basin-wide macro-nutrient limitation to some degree. When the aeolian iron supply is enhanced (the high dust case) the Atlantic becomes more macro-nutrient limited, basin wide phosphate concentrations decrease, and phosphorus accumulates in the other basins.

5. Discussion and Conclusion

[60] We have used an ocean circulation model with an embedded ecosystem and iron parameterization to examine the interactions between supplies of macro-nutrients, iron, and productivity. We have used idealized (uniform) dust fluxes to force the system to iron replete and iron starved oceans. This simplistic iron forcing was chosen to show the results clearly. Qualitatively, the same results are obtained when experiments with realistic patterns, but lower and higher magnitudes of aeolian iron fluxes, were used. Our sensitivity experiments have shown the importance not only of upwelling of nutrients, but also of the lateral advection and the unique interplay between macro-nutrient and iron supply to the upper ocean.

[61] We used the basic state, and sensitivity experiments with the numerical model to illustrate the following conceptual view of how these interactions control the modern ocean.

[62] 1. The modern ocean may be considered as composed of (1) oligotrophic gyres which are macro-nutrient limited, (2) upwelling regions which are iron limited, and (3) upwelling regions which are iron replete.

[63] 2. The productivity of the oligotrophic gyres is sustained, on the long term, by lateral transfer of nutrients from the surrounding upwelling regions.

[64] 3. There is a global scale analogy in which the Atlantic macro-nutrient loading and productivity is controlled by the relative iron stress of the Southern Ocean and upwelling regions in the Indo-Pacific.

[65] 4. As a consequence, the sensitivity to increased aeolian iron supply changes from basin to basin. In response to enhanced dust fluxes, the following occurs. (1) In the Southern Ocean and Indo-Pacific the upwelling regions are (partially) relieved of iron stress and become more productive. (2) This leads to weakened lateral transport of macro-nutrients in the upper ocean, decreasing productivity in the oligotrophic regions of the Indo-Pacific and over the whole of the Atlantic basin.

[66] An important finding here was that there is an asymmetry in the response to decreased and increased aeolian iron supply (Figure 10 and Table 2), with a dramatic response when iron fluxes were halved, and a much smaller response to even significantly larger iron fluxes. Another inference of this model study is that in a higher dust world, the size of the oligotrophic regions will increase. More intense productivity will occur near the sites of macro-nutrient upwelling, reducing the macro-nutrients transported laterally, and less productivity will occur in the subtropical gyres. With a weaker aeolian iron supply, more macro-nutrients reach the subtropical gyres, and there will be more uniform, low production throughout the surface ocean (Figure 14).

[67] The study also suggests a strong contrast between the behavior of the Atlantic and Indo-Pacific sensitivities owing to differences in their overturning circulation (and apart from their modern iron replete and deplete natures). Macro-nutrients are supplied by upper ocean inflow to the Atlantic basin, and exported at depth. In a dustier world, higher productivity elsewhere in the ocean reduces the surface macro-nutrient concentrations and the lateral supply to the Atlantic Ocean. The Atlantic becomes more macro-nutrient stressed and uniformly less productive.

[68] This has some interesting consequences for hypothesis relating iron limitation of nitrogen fixing organisms. Diazotrophs have a high iron requirement [*Berman-Frank et al.*, 2001; *Sañudo-Wilhelmy et al.*, 2001], and it appears that these organisms may be iron limited even in relatively iron rich regions of the ocean [*Mills et al.*, 2004]. Following this train of thought, it has been suggested that relief of iron limitation might stimulate nitrogen fixation, relieving global nitrogen limitation and enhancing the biological pumps of carbon [*Falkowski*, 1997]. However, though we do not represent nitrogen cycle dynamics here, we suggest that for the Atlantic basin, global scale iron fertilization of nitrogen fixation could be counterbalanced by the reduction of available phosphorus.

[69] While the details of our results are dependent on the specifics of the model, the general patterns of sensitivity are robust over a wide range of model parameters. We have performed the same sensitivity experiments on several versions of the model using different ecosystem parameters. All sets of experiments show the same qualitative sensitivity results. Future studies will address the impact of varying iron solubilities and ligand concentrations that likely occur in the ocean. These may alter specifics of our results, but we expect the overall patterns to be robust. In order to perform a number of equilibrium spinup studies with the model at global scale, we have not resolved the role of meso-scale features. While eddy pumping may support a significant fraction of subtropical new production [*McGillicuddy et al.*, 1998], it only redistributes nutrients within the bowl of the gyre. Lateral eddy transfer of nutrients, near the surface and between upwelling and downwelling regimes, may significantly reinforce the important Ekman supply and help to balance the loss of nutrient from the base of the bowl of the thermocline (Figure 12). *Oschlies* [2002] showed that in a numerical model, lateral eddy nutrient supply to the euphotic zone is important, especially near the subtropical boundaries. *Kawamiya* [2001] also found that mesoscale transport could be crucial for maintaining nutrient budgets. We anticipate that resolving eddies will not change the main results found in this study, but it will be interesting to investigate how some of the details may be affected.

[70] We have shown that it is important to consider the three-dimensional nature of macro-nutrient supply in the oceans, especially when considering long-term budgets. A one-dimensional view of macro-nutrient supply in the subtropics and the Atlantic is valid on a year-to-year basis, but lateral supply dominates the nutrient budgets of these regions on longer timescales. Our studies show the intricate interplay between iron supply and macro-nutrient supply over larger tracts of the world's oceans. Changes in iron deposition will have profound effects on macro-nutrient supplies in regions where the long-term budgets of macro-nutrients are dictated by lateral supply.

[71] These results have implications for the debate about deliberate iron fertilization of the oceans, an idea proposed as a means to mitigate human induced increase in atmospheric CO_2. Fertilization in one area will have important consequences in other regions. A fertilized Southern Ocean will affect the supply of macro-nutrients to the southern subtropical gyres, with perhaps the consequence of reduced productivity in these regions. Large-scale fertilization will also affect nutrient supply to the North Atlantic, with the potential for reducing production there, too.

[72] Here we have discussed the change caused by increased/decreased productivity due to iron deposition. However, the consequences of changes to productivity by other factors, such as increased stratification, longer growing season (e.g., in future climate change scenarios [*Bopp et al.*, 2001]), may also be significant, especially in reference to nonlocal responses engendered by lateral supply of nutrients. Speculations about near-future climate change have also suggested a slowing down of deep water formation due to the freshing and warming of the North Atlantic (e.g., almost all the models in the Coupled Model Intercomparison Project, CMIP [*Covey et al.*, 2003]). This would have an effect on the upper ocean inflow into the Atlantic, perhaps reducing macro-nutrient supply and North Atlantic productivity. However, a warmer, wetter climate may also mean a reduction in the aeolian iron supply. How will these two interplay along with other changes to productivity by a more stratified ocean?

[73] We have presented a physical-biogeochemical model of intermediate complexity which we have used to explore

aspects of the three-dimensional nutrient supply to the euphotic zone. We have reinforced and illustrated the importance of two lateral supply mechanisms, (1) Ekman transport of nutrients from upwelling regions into subtropical gyres to compensate for the slow leak of nutrients from the base of the gyre bowl, and (2) upper ocean flow into the Atlantic supplying the nutrients that are slowly leaked out of the Atlantic by North Atlantic Deep Water.

[74] We suggest that a change to the productivity in upwelling regions of the ocean (due here to changes to the iron deposition) will change the amount of nutrients transported "downstream," altering the productivity of the Atlantic basin and the Indo-Pacific subtropical gyres. The global macro-nutrient and iron cycles and biological productivity are intimately linked through the complex, three-dimensional circulation.

Appendix A

A1. Ecosystem Model Equations and Parameters

[75] We present here the symbols and equations used in the ecosystem model described in 2.3. There are three nutrient pools: PO_4, phosphate; Si, silicic acid; and Fe_T, dissolved inorganic iron (free + ligand bound). The plankton pools are: Q_1, small phytoplankton; Q_2, diatoms; and Z, zooplankton; we use the subscripts p, fe to denote the phosphorus or iron content of these classes. Silicon and iron contents of Q_1 and Q_2 are in constant ratio to phosphorus, and we assume no silicon content in zooplankton.

[76] Detrital organic matter divides into two pools: DOM, dissolved organic matter; and POM, particulate organic matter. We use the subscripts p, si, and fe to denote the phosphorus, silicon, or iron content of these pools. There is no DOM pool of silicon. The ratio of the partitioning between pools is defined by λ. The subscripts on the λ's used below are m for organic matter produced by mortality and excretion and g produced by sloppy feeding. Additional variables are given by the following symbols: I, photosynthetically available radiation (PAR); Fe', free iron; and F_{atmos}, aeolian deposition of iron.

[77] The model parameter values used in this model are given in Table 1 and are discussed below. All tracer tendency terms also include effects of advection and diffusion by the circulation model; the equations below denote only the biological and chemical source/sink term (and sedimentation and aeolian deposition in the case of iron), S_A of equation (2).

$$\frac{dPO_4}{dt} = -\mu_{q_1} Q_{1_p} - \mu_{q_2} Q_{2_p} + r_p DOM_p + r_p POM_p,$$

$$\frac{dQ_{1_p}}{dt} = \mu_{q_1} Q_{1_p} - m_{q_1}\left(Q_{1_p} - Q_e\right) - g_{q_1} Z_p,$$

$$\frac{dQ_{2_p}}{dt} = \mu_{q_2} Q_{2_p} - m_{q_2}\left(Q_{2_p} - Q_e\right) - g_{q_2} Z_p,$$

$$\frac{dZ_p}{dt} = \gamma_{q_1} g_{q_1} Z_p + \gamma_{q_2} g_{q_2} Z_p - m_z\left(Z_p - Z_e\right),$$

$$\begin{aligned}\frac{dDOM_p}{dt} = {} & \lambda_{mq_1} m_{q_1}\left(Q_{1_p} - Q_e\right) \\ & + \lambda_{mq_2} m_{q_2}\left(Q_{2_p} - Q_e\right) + \lambda_{mz} m_z\left(Z_p - Z_e\right) \\ & + \lambda_g\left[\left(1-\gamma_{q_1}\right) g_{q_1} Z_p + \left(1-\gamma_{q_2}\right) g_{q_2} Z_p\right] \\ & - r_p DOM_p,\end{aligned}$$

$$\begin{aligned}\frac{dPOM_p}{dt} = {} & \left(1-\lambda_{mq_1}\right) m_{q_1}\left(Q_{1_p} - Q_e\right) \\ & + \left(1-\lambda_{mq_2}\right) m_{q_2}\left(Q_{2_p} - Q_e\right) \\ & + \left(1-\lambda_{mz}\right) m_z\left(Z_p - Z_e\right) \\ & + \left(1-\lambda_g\right)\left[\left(1-\gamma_{q_1}\right) g_{q_1} Z_p\right. \\ & \left. + \left(1-\gamma_{q_2}\right) g_{q_2} Z_p\right] \\ & - w_p \frac{dPOM_p}{dz} - r_p POM_p,\end{aligned}$$

$$\frac{dSi}{dt} = -R_{(si:p)_{q_2}}\left[\mu_{q_2} Q_{2_p}\right] + r_{si} POM_{si},$$

$$\begin{aligned}\frac{dPOM_{si}}{dt} = {} & R_{(si:p)_{q_2}}\left[m_{q_2}\left(Q_{2_p} - Q_e\right) + g_{q_2} Z_p\right] - w_{si}\frac{dPOM_{si}}{dz} \\ & - r_{si} POM_{si},\end{aligned}$$

$$\begin{aligned}\frac{dFe_T}{dt} = {} & -R_{(fe:p)_{q_1}}\left[\mu_{q_1} Q_{1_p}\right] - R_{(fe:p)_{q_2}}\left[\mu_{q_2} Q_{2_p}\right] \\ & + r_{fe} DOM_{fe} + r_{fe} POM_{fe} \\ & - \kappa_s Fe' + \alpha F_{atmos},\end{aligned}$$

$$\frac{dZ_{fe}}{dt} = R_{(fe:p)_{q_1}}\left[\gamma_{q_1} g_{q_1} Z_p\right] + R_{(fe:p)_{q_2}}\left[\gamma_{q_2} g_{q_2} Z_p\right] - m_z Z_{fe},$$

$$\begin{aligned}\frac{dDOM_{fe}}{dt} = {} & R_{(fe:p)_{q_1}}\left[\lambda_{mq_1} m_{q_1}\left(Q_{1_p} - Q_e\right)\right. \\ & \left. + \lambda_g\left(1-\gamma_{q_1}\right) g_{q_1} Z_p\right] \\ & + R_{(fe:p)_{q_2}}\left[\lambda_{mq_2} m_{q_2}\left(Q_{2_p} - Q_e\right)\right. \\ & \left. + \lambda_g\left(1-\gamma_{q_2}\right) g_{q_2} Z_p\right] \\ & + \lambda_{mz} m_z Z_{fe} - r_{fe} DOM_{fe},\end{aligned}$$

$$\begin{aligned}\frac{dPOM_{fe}}{dt} = {} & R_{(fe:p)_{q_1}}\left[\left(1-\lambda_{mq_1}\right) m_{q_1}\left(Q_{1_p} - Q_e\right)\right. \\ & \left. + \left(1-\lambda_g\right)\left(1-\gamma_{q_1}\right) g_{q_1} Z_p\right] \\ & + R_{(fe:p)_{q_2}}\left[\left(1-\lambda_{mq_2}\right) m_{q_2}\left(Q_{2_h} - Q_e\right)\right. \\ & \left. + \left(1-\lambda_g\right)\left(1-\gamma_{q_2}\right) g_{q_2} Z_p\right] \\ & + \left(1-\lambda_{mz}\right) m_z Z_{fe} \\ & - w_{fe}\frac{dPOM_{fe}}{dz} - r_{fe} POM_{fe},\end{aligned}$$

where

$$\mu_{q_1} = \mu_{o_{q_1}} \frac{I}{I + (I)_{q_1}} \min\left(\frac{PO_4}{PO_4 + (PO_4)_{q_1}}, \frac{Fe_T}{Fe_T + (Fe)_{q_1}}\right),$$

$$\mu_{q_2} = \mu_{o_{q_2}} \frac{I}{I + (I)_{q_2}} \min\left(\frac{PO_4}{PO_4 + (PO_4)_{q_2}}, \frac{Si}{Si + (Si)_{q_2}}, \frac{Fe_T}{Fe_T + (Fe)_{q_2}}\right),$$

$$g_{q_1} = g_o \frac{\eta_{q_1} Q_1}{A} \frac{A - Q_o}{A - Q_o + (Q)_z},$$

$$g_{q_2} = g_o \frac{\eta_{q_2} Q_2}{A} \frac{A - Q_o}{A - Q_o + (Q)_z},$$

$$A = \eta_{q_1} Q_1 + \eta_{q_2} Q_2,$$

and free iron concentration (Fe') is calculated from the equilibrium solution,

$$Fe' + L' \Longleftrightarrow^{k_f}_{k_d} FeL,$$
$$Fe_T = Fe' + FeL,$$
$$L_T = L' + FeL,$$

with $\beta = \frac{k_f}{k_d}$ representing ligand binding strength, where k_f is the forward rate constant and k_d is the reverse rate constant, and with L_T representing total organic ligand (constant).

[78] Chlorophyll, *Chl*, is calculated from the phosphorus content of phytoplankton in a similar manner to *Doney et al.* [1996],

$$Chl = Q_{1_p}\left[B^{\max} - \left(B^{\max} - B^{\min}\right)\min\left(\frac{I}{I_*}, 1\right)\right] \min\left(\frac{PO_4}{PO_4 + (PO_4)_{q_1}}, \frac{Fe_T}{Fe_T + (Fe)_{q_1}}\right) + Q_{2_p}\left[B^{\max} - \left(B^{\max} - B^{\min}\right)\min\left(\frac{I}{I_*}, 1\right)\right] \min\left(\frac{PO_4}{PO_4 + (PO_4)_{q_2}}, \frac{Si}{Si + (Si)_{q_2}}, \frac{Fe_T}{Fe_T + (Fe)_{q_2}}\right).$$

Here $B^{\max}$ and $B^{\min}$ are maximum and minimum chlorophyll to phosphorus ratio and I_* is critical irradiance for photoadaptation.

A2. Parameter Values

[79] Parameters used for the control run are given in Table 1. Wherever possible, values are chosen from within the range provided by experimental and modeling literature.

[80] Estimates of maximum phytoplankton growth rates ($\mu_{o_{q1}}$, $\mu_{o_{q2}}$) lie between $\frac{1}{2}$ and $\frac{1}{0.25}$ d^{-1} [*Eppley*, 1972; *Eppley and Renger*, 1974]. Diatoms typically grow quicker than small phytoplankton [e.g., *Liu et al.*, 2002]. The rates we chose here are within the range of similar models [e.g., *Gregg et al.*, 2003]. Zooplankton grazing rate (g_o) and plankton mortality rates (m_{q_1}, m_{q_2}, m_z) are difficult to determine experimentally. Often these are used as free parameters in models [e.g., *Fasham et al.*, 1990]. We chose grazing rates within the range used in similar models [e.g., *Gregg et al.*, 2003; *Chai et al.*, 2002]. In this model, the mortality term also incorporates excretion; these are often separate in other models (especially nitrogen based models which resolve ammonium) and we chose rates that are on the high end of the range chosen by other models [e.g., *Moore et al.*, 2002a; *Aumont et al.*, 2003].

[81] The half-saturation light constant (I_{q_1}, I_{q_2}) varies between species of phytoplankton and has been measured within the range 5 to 100 W m^{-2} [*Parson et al.*, 1990; *Sakshaug and Slagstad*, 1991; *Rhee and Gotham*, 1981]. Half-saturation rates of phosphate ($PO_{4_{q1}}$, $PO_{4_{q2}}$), silicic acid (Si_{q_2}), and iron (Fe_{q_1}, Fe_{q_2}) are chosen following experimentally based estimates, and are similar to those used in other models. We base our phosphate half-saturation constants on other model studies using phosphorus as the main currency [e.g., *Aumont et al.*, 2003; *Lancelot et al.*, 2000], and with Redfield ratio of those using nitrogen [e.g., *Gregg et al.*, 2003; *Chai et al.*, 2002]. Silicic acid half-saturation has been found to vary across the ocean, from as low as 0.5 μM in the Gulf Stream [*Brzezinski and Nelson*, 1989] to much higher (greater than 4 μM) in the Southern Ocean [*Pondaven et al.*, 1999]. We chose a value within this range. Iron half saturation values have been measured as fairly low [e.g., *Price et al.*, 1994] for communities composed of small phytoplankton, and higher [e.g., *Fitzwater et al.*, 1996] for communities which also contain diatoms. The half-saturation of phytoplankton in grazing rates is difficult to measure experimentally. Here we use a value within the range of similar models [e.g., *Aumont et al.*, 2003; *Loukos et al.*, 1997].

[82] Ratios of silicon to phosphorus in diatom cells ($R_{(si:p)_{q2}}$) vary, especially between iron-replete and iron-deplete regions [*Franck et al.*, 2000]. For the purpose of this study we use a constant value that falls in the range found observationally [*Brzezinski*, 1985] (and using Redfield ratio to convert N:P; [*Sunda et al.*, 1991; *Sunda and Huntsman*, 1995]). Iron to phosphorus values ($R_{(fe:p)_{q1}}$, $R_{(fe:p)_{q2}}$) vary regionally and between species. Ratios as low as 2×10^{-4} and as high as 1.3×10^{-3} [*Sunda*, 1997] (conversion from Fe:C to Fe:P done through Redfield ratio) have been measured. We chose a higher ratio for diatoms than for small phytoplankton following *Lancelot et al.* [2000].

[83] We use a grazing efficiency value typical of other models [e.g., *Moore et al.*, 2002a]. The grazing rate parameterization follows *Evans* [1988], and we use the values of phytoplankton palatability to the zooplankton (η_{q_1}, η_{q_2}), used in that study. Threshold grazing (Q_o) and plankton minimum concentrations (Q_e, Z_e) are very small, and help in

maintaining at least seed amounts of plankton in any grid cell.

[84] Observations [e.g., *Hansell and Waterhouse*, 1997] suggest that a significant fraction (about half) of net community production forms "semi-labile" *DOM*. We use the parameter λ to determine the ratio of biological matter entering *DOM* and *POM*. These values differ for organic material from different plankton (λ_{mq_1}, λ_{mq_2}, λ_{mz}) and for material from sloppy feeding (λ_g). Modeling studies suggest that the remineralization rate of semi-labile *DOM* is of order weeks to months [e.g., *Archer et al.*, 1997; *Yamanaka and Tajika*, 1997]. We use the same rate (r_p, r_{si}, r_{fe}) for dissolved and particulate pools, and so chose relatively long rates, but still within range of other models [e.g., *Aumont et al.*, 2003; *Leonard et al.*, 1999]. *Johnson et al.* [1997] suggest that remineralization rates for phosphorus and iron in *POM* are relatively similar, so we treat these two the same. Silicon has a much longer remineralization time [*Tréguer et al.*, 1995]. Sinking speeds are taken as slower for iron and phosphorus (w_p, w_{fe}), and faster for silicon (w_{si}), following *Chai et al.* [2002]. Speeds are similar to those used in similar models [*Gregg et al.*, 2003; *Chai et al.*, 2002].

[85] Recent studies [*Jickells and Spokes*, 2001; *Duce and Tindale*, 1991] suggest that the solubility of iron (α) is between 1 and 10%. The iron scavenging rates (κ_s), ligand binding strength (β), and uniform organic ligand concentration (L) are taken from the sensitivity modeling study of *Parekh et al.* [2004]. There are no direct measurements of iron scavenging rates, and ligand strength and concentrations are within the range found by *Gledhill and van den Berg* [1994], *van den Berg* [1995], *Rue and Bruland* [1995], and *Rue and Bruland* [1997]. The parameters to convert phosphorus in phytoplankton to chlorophyll ($B^{\max}$, $B^{\min}$, I_*) follow those used by *Aumont et al.* [2003].

[86] **Acknowledgments.** We would like to thank Takamitsu Ito for helpful discussions and Natalie Mahowald for providing the dust forcing fields. Jorge Sarmiento and an anonymous reviewer provided valuable suggestions and comments. This work was supported in part by PARADIGM NOPP (N000014-02-1-0370), NOAA (NA16GP2988), and NSF (OCE-0350672). P. P. is also grateful to the NASA Earth System Science Fellowship Program (NGT5-30362) for funding.

References

Antoine, D., J. M. André, and A. Morel (1996), Oceanic primary production: 2. Estimation of global scale from satellite (CZCS) chlorophyll, *Global Biogeochem. Cycles*, *10*, 57–69.

Archer, D., and E. K. Johnson (2000), A model of the iron cycle in the ocean, *Global Biogeochem. Cycles*, *14*, 269–279.

Archer, D., E. T. Peltzer, and D. L. Kichman (1997), A timescale for dissolved organic carbon production in equatorial Pacific surface waters, *Global Biogeochem. Cycles*, *11*, 435–452.

Archer, D., A. Winguth, D. Lea, and N. Mahowald (2000), What caused the glacial/interglacial atmospheric pCO_2 cycles?, *Rev. Geophys.*, *38*, 159–189.

Aumont, O., J. Orr, P. Monfray, G. Madec, and E. Maier-Reimer (1999), Nutrient trapping in the equatorial Pacific: The ocean circulation solution, *Global Biogeochem. Cycles*, *13*, 351–369.

Aumont, O., E. Maier-Reimer, S. Blain, and P. Monfray (2003), An ecosystem model of the global ocean including Fe, Si, P co-limitation, *Global Biogeochem. Cycles*, *17*(2), 1060, doi:10.1029/2001GB001745.

Banse, K. (1992), Grazing, temporal changes of phytoplankton concentrations, and the microbial loop in the open sea, in *Primary Productivity and Biogeochemical Cycles in the Sea*, edited by P. G. Falkowski and A. D. Woodhead, pp. 409–440, Springer, New York.

Behrenfeld, M. J., and P. G. Falkowski (1997), A consumer's guide to phytoplankton primary productivity models, *Limnol. Oceanogr.*, *42*, 1479–1491.

Berman-Frank, I., J. T. Cullen, Y. Shaked, R. M. Sherrell, and P. G. Falkowski (2001), Iron availability, cellular iron quotas, and nitrogen fixation in *Trichodesmium*, *Limnol. Oceanogr.*, *46*, 1249–1260.

Bopp, L., P. Monfray, O. Aumont, J.-L. Dufresne, H. le Treut, G. Madec, L. Terray, and J. C. Orr (2001), Potential impact of climate change in marine export production, *Global Biogeochem. Cycles*, *15*, 81–99.

Bopp, L., K. Kohfeld, and C. Le Quéré (2003), Dust impact on marine biota and atmospheric CO_2, *Paleogeography*, *18*(2), 1046, doi:10.1029/20002PA000081.

Boyd, P. W., et al. (2000), A mesoscale phytoplankton bloom in the polar Southern Ocean stimulated by iron fertilization, *Nature*, *407*, 695–702.

Boye, M. C., M. G. van den Berg, J. T. M. deJong, H. Leach, P. Croot, and H. J. W. de Baar (2001), Organic complexation of iron in the Southern Ocean, *Deep Sea Res., Part I*, *48*, 1477–1497.

Boye, M., A. P. Aldrich, C. M. G. van den Berg, J. T. M. de Jong, M. Veldhuis, and H. J. W. de Baar (2003), Horizontal gradient of the chemical speciation of iron in surface waters of the northeast Atlantic Ocean, *Mar. Chem.*, *80*, 129–143.

Bruland, K. W., K. J. Orians, and J. P. Cowen (1994), Reactive trace metals in the stratified central North Pacific, *Geochem. Cosmochim. Acta*, *58*, 3171–3182.

Brzezinski, M. A. (1985), The Si:C:N ratio of marine diatoms: Interspecific variability and the effect of some environmental variables, *J. Phycol.*, *21*, 347–357.

Brzezinski, M. A., and D. M. Nelson (1989), Seasonal changes in the silicon cycling within a Gulf Stream warm-core ring, *Deep Sea Res., Part I*, *36*, 1009–1030.

Brzezinski, M. A., C. J. Pride, V. M. Franck, D. M. Sigman, J. L. Sarmiento, K. Matsumoto, N. Gruber, G. H. Rau, and K. H. Coale (2002), A switch from Si $(OH)_4$ to NO_3^- depletion in the glacial Southern Ocean, *Geophys. Res. Lett.*, *29*(12), 1564, doi:10.1029/2001GL014349.

Chai, F., R. C. Dugdale, T.-H. Peng, F. P. Wilkerson, and R. T. Barber (2002), One-dimensional ecosystem model of the equatorial Pacific upwelling system: I. Model development and silicon and nitrogen cycle, *Deep Sea Res., Part II*, *49*, 2713–2745.

Christian, J. R., M. A. Verschell, R. Murtugudde, A. J. Busalacchi, and C. R. McClain (2002), Biogeochemical modelling of the tropical Pacific Ocean: II. Iron biogeochemistry, *Deep Sea Res., Part II*, *49*, 545–565.

Coale, K. H., et al. (1996), A massive phytoplankton bloom induced by an ecosystem-scale iron fertilization experiment in the equatorial Pacific Ocean, *Nature*, *383*, 495–501.

Conkright, M. E., H. E. Garcia, T. D. O'Brien, R. A. Locarnini, T. P. Boyer, C. Stephens, and J. I. Antonov (2002), *World Ocean Atlas 2001*, vol. 4, *Nutrients*, *NOAA Atlas NESDIS 52*, Natl. Oceanic and Atmos. Admin., Silver Spring, Md.

Covey, C., K. M. AchutaRao, U. Cubasch, P. Jones, S. J. Lambert, M. E. Mann, T. J. Phillips, and K. E. Taylor (2003), An overview of results from the Coupled Model Intercomparison Project (CMIP), *Global Planet. Change*, *37*, 103–133.

de Baar, H. J. W., J. T. M. de Jong, R. F. Nolting, K. R. Timmermans, M. A. van Leeuwe, U. Bathmann, M. Rutgers van der Loeff, and J. Sildam (1999), Low dissolved Fe and the absence of diatom blooms in the remote Pacific waters of the Southern Ocean, *Mar. Chem.*, *66*, 1–34.

Doney, S. C., D. M. Glover, and R. G. Najjar (1996), A new coupled one-dimensional biological-physical model for the upper ocean: Applications to the JGOFS Bermuda Atlantic Time-series Study (BATS) site, *Deep Sea Res., Part II*, *43*, 591–634.

Duce, R., and N. Tindale (1991), Atmospheric transport of iron and its deposition in the ocean, *Limnol. Oceanogr.*, *36*, 1715–1726.

Dutay, J.-C., et al. (2002), Evaluation of ocean model ventilation with CFC-11: Comparison of 13 global ocean models, *Ocean Modell.*, *4*, 89–120.

Dutkiewicz, S., M. Follows, J. Marshall, and W. W. Gregg (2001), Interannual variability of phytoplankton abundances in the North Atlantic, *Deep Sea Res., Part II*, *48*, 2323–2344.

Elrod, V. A., W. M. Berelson, K. H. Coale, and K. S. Johnson (2004), The flux of iron from continental shelf sediments: A missing source for global budgets, *Geophys. Res. Lett.*, *31*, L12307, doi:10.1029/2004GL020216.

Eppley, R. W. (1972), Temperature and phytoplankton growth in the sea, *Fish. Bull.*, *70*, 1063–1085.

Eppley, R. W., and B. J. Peterson (1979), Particulate organic matter flux and planktonic new production in the deep ocean, *Nature*, *282*, 677–680.

Eppley, R. W., and E. M. Renger (1974), Nitrogen assimilation of an oceanic diatom in nitrogen-limited continuous culture, *J. Phycol.*, *18*, 534–551.

Evans, G. T. (1988), A framework for discussing seasonal succession and coexistence of phytoplankton species, *Limnol. Oceanogr.*, *33*, 1027–1036.

Falkowski, P. G. (1997), Evolution of the nitrogen cycle and its influence on the biological sequestration of CO_2 in the ocean, *Nature*, *387*, 272–275.

Falkowski, P. G., D. Ziemann, Z. Kolber, and P. K. Bienfang (1991), Role of eddy pumping in enhancing primary production in the ocean, *Nature*, *352*, 55–58.

Fasham, M. J. R. (1995), Variations in the seasonal cycle of biological production in subarctic oceans: A model sensitivity analysis, *Deep Sea Res., Part I*, *42*, 1111–1149.

Fasham, M. J. R., H. W. Ducklow, and S. M. McKelvie (1990), A nitrogen-based model of plankton dynamics in the oceanic mixed layer, *J. Mar. Res.*, *48*, 591–639.

Fitzwater, S. E., K. H. Coale, R. M. Gordon, K. S. Johnson, and M. E. Ondrusek (1996), Iron deficiency and phytoplankton growth in the equatorial Pacific, *Deep Sea Res., Part II*, *43*, 995–1015.

Franck, V. M., M. A. Brzezinski, K. H. Coale, and D. M. Nelson (2000), Iron and silicic acid concentrations regulate Si uptake north and south of the Polar Frontal Zone in the Pacific Sector of the Southern Ocean, *Deep Sea Res., Part II*, *47*, 3315–3338.

Fung, I. Y., S. K. Meyn, I. Tegen, S. Doney, J. John, and J. Bishop (2000), Iron supply and demand in the upper ocean, *Global Biogeochem. Cycles*, *14*, 281–295.

Ganachaud, A., and C. Wunsch (2000), The oceanic meridional overturning circulation, mixing, bottom water formation and heat transport, *Nature*, *408*, 453–457.

Gao, Y., S. Fan, and J. L. Sarmiento (2003), Aeolian iron input to the ocean through precipitation scavenging: A modeling perspective and its implication for natural iron fertilization in the ocean, *J. Geophys. Res.*, *108*(D7), 4221, doi:10.1029/2002JD002420.

Gent, P., and J. McWilliams (1990), Isopycnal mixing in ocean circulation models, *J. Phys. Oceanogr.*, *20*, 150–155.

Gledhill, M., and C. van den Berg (1994), Determination of complexation of iron (III) with natural organic complexing ligands in seawater using cathodic stripping voltammetry, *Mar. Chem.*, *47*, 41–54.

Gnanadesikan, A. (1999), A global model of silicon cycling: Sensitivity to eddy parameterization and dissolution, *Global Biogeochem. Cycles*, *13*, 199–220.

Gnanadesikan, A., and J. R. Toggweiler (1999), Constraints placed by silicon cycling on vertical exchange in general circulation models, *Geophys. Res. Lett.*, *26*, 1865–1868.

Gnanadesikan, A., R. D. Slater, N. Gruber, and J. L. Sarmiento (2002), Oceanic vertical exchange and new production: A comparison between models and observations, *Deep Sea Res., Part II*, *49*, 363–401.

Gordon, R. M., K. H. Coale, and K. S. Johnson (1997), Iron distributions in the equatorial Pacific: Implications for new production, *Limnol. Oceanogr.*, *42*, 419–431.

Gregg, W., P. Ginoux, P. Schopf, and N. Casey (2003), Phytoplankton and iron: Validation of a global three-dimensional ocean biogeochemical model, *Deep Sea Res., Part II*, *50*, 3143–3169.

Hansell, D. A., and T. Y. Waterhouse (1997), Controls on the distributions of organic carbon and nitrogen in the eastern Pacific Ocean, *Deep Sea Res., Part I*, *44*, 843–857.

Ito, T., J. Marshall, and M. J. Follows (2004), What controls the uptake of transient tracers in the southern ocean?, *Global Biogeochem. Cycles*, *18*, GB2021, doi:10.1029/2003GB002103.

Jenkins, W. J., and S. C. Doney (2003), The subtropical nutrient spiral, *Global Biogeochem. Cycles*, *17*(4), 1110, doi:10.1029/2003GB002085.

Jiang, S., P. H. Stone, and P. Malanotte-Rizzoli (1999), An assessment of the Geophysical Fluid Dynamics Laboratory ocean model with coarse resolution: Annual-mean climatology, *J. Geophys. Res.*, *104*, 25,623–25,645.

Jickells, T. D., and L. J. Spokes (2001), Atmospheric iron inputs to the oceans, in *The Biogeochemistry of Iron in Seawater*, edited by D. R. Turner and K. A. Hunter, pp. 85–121, John Wiley, Hoboken, N. J.

Johnson, K. S., R. M. Gordon, and K. H. Coale (1997), What controls dissolved iron concentrations in the world ocean?, *Mar. Chem.*, *57*, 137–161.

Johnson, K. S., et al. (2003), Surface ocean-lower atmosphere interactions in the Northeast Pacific Ocean gyre: Aerosols, iron, and the ecosystem response, *Global Biogeochem. Cycles*, *17*(2), 1063, doi:10.1029/2002GB002004.

Kawamiya, M. (2001), Mechanism of offshore nutrient supply in the western Arabian Sea, *J. Mar. Res.*, *59*, 675–696.

Kutzbach, J. E., and R. G. Gallimore (1989), Pangean climates: Megamonsoons of the megacontinent, *J. Geophys. Res.*, *94*, 3341–3357.

Lancelot, C., E. Hannon, S. Becquevort, C. Veth, and H. J. W. De Baar (2000), Modeling phytoplankton blooms and carbon export production in the Southern Ocean: Dominant controls by light and iron in the Atlantic sector in Austral spring 1992, *Deep Sea Res., Part I*, *47*, 1621–1662.

Laws, E. A., P. G. Falkowski, W. O. Smith, H. Ducklow, and J. J. McCarthy (2000), Temperature effects on export production in the open ocean, *Global Biogeochem. Cycles*, *14*, 1231–1246.

Lee, M.-M., D. P. Marshall, and R. G. Williams (1997), On the eddy transfer of tracers: Advective or diffusive, *J. Mar. Res.*, *55*, 483–505.

Leonard, C. L., C. R. McClain, R. Murtugudde, E. E. Hofmann, and L. W. Harding Jr. (1999), An iron-based ecosystem model of the central equatorial Pacific, *J. Geophys. Res.*, *104*, 1325–1341.

Levitus, S., and T. P. Boyer (1994), *World Ocean Atlas 1994*, vol. 4, *Temperature*, NOAA Atlas NESDIS 4, 117 pp., Natl. Oceanic and Atmos. Admin., Silver Spring, Md.

Levitus, S., R. Burgett, and T. P. Boyer (1994), *World Ocean Atlas 1994*, vol. 3, *Salinity*, *NOAA Atlas NESDIS 3*, 99 pp., Natl. Oceanic and Atmos. Admin., Silver Spring, Md.

Lévy, M., P. Klein, and A.-M. Treguier (2001), Impact of sub-mesoscale physics on production and subduction of phytoplankton in an oligotrophic regime, *J. Mar. Res.*, *59*, 535–565.

Liu, H., K. Suzuki, and T. Saino (2002), Phytoplankton growth and microzooplankton grazing in the subarctic Pacific Ocean and the Bering Sea during summer 1999, *Deep Sea Res., Part I*, *49*, 363–375.

Longhurst, A., S. Sathyendranath, T. Platt, and C. Caverhill (1995), An estimate of global primary production in the ocean from satellite radiometer data, *J. Plankton Res.*, *17*, 1245–1271.

Loukos, H., B. Frost, D. E. Harrison, and J. W. Murray (1997), An ecosystem model with iron limitation of primary production in the equatorial Pacific at 140°W, *Deep Sea Res., Part II*, *44*, 2221–2249.

Mackey, D. J., J. E. O'Sullivan, and R. J. Watson (2002), Iron in the western Pacific: A riverine or hydrothermal source for iron in the Equatorial Undercurrent, *Deep Sea Res., Part I*, *49*, 877–893.

Mahadevan, A., and D. Archer (2000), Modelling the impact of fronts and mesoscale circulation on the nutrient supply and biogeochemistry of the upper ocean, *J. Geophys. Res.*, *105*, 1209–1225.

Mahowald, N., K. Kohfeld, M. Hansson, Y. Balkanski, S. Harrison, I. Prentice, M. Schultz, and H. Rodhe (1999), Dust sources and deposition during the Last Glacial Maximum and current climate: A comparison of model results with paleodata from ice cores and marine sediments, *J. Geophys. Res.*, *104*, 15,895–15,916.

Mahowald, N., C. Lou, J. del Corral, and C. Zender (2003), Interannual variability in atmospheric mineral aerosols from a 22-year model simulation and observational data, *J. Geophys. Res.*, *108*(D12), 4352, doi:10.1029/2002JD002821.

Marshall, J. C., C. Hill, L. Perelman, and A. Adcroft (1997a), Hydrostatic, quasi-hydrostatic and non-hydrostatic ocean modeling, *J. Geophys. Res.*, *102*, 5733–5752.

Marshall, J. C., A. Adcroft, C. Hill, L. Perelman, and C. Heisey (1997b), A finite-volume, incompressible Navier-Stokes model for the studies of the ocean on parallel computers, *J. Geophys. Res.*, *102*, 5753–5766.

Martin, J. (1990), Glacial-interglacial CO_2 change: The iron hypothesis, *Paleogeography*, *5*, 1–13.

Martin, J. H., and S. Fitzwater (1988), Iron deficiency limits phytoplankton growth in the north-east Pacific subarctic, *Nature*, *331*, 341–343.

Martin, J., G. Knauer, D. Karl, and W. Broenkow (1987), VERTEX: Carbon cycling in the northeast Pacific, *Deep Sea Res.*, *34*, 267–285.

Martin, J. H., et al. (1994), Testing the iron hypothesis in ecosystems of the equatorial Pacific Ocean, *Nature*, *371*, 123–129.

Matsumoto, K., J. L. Sarmiento, and M. A. Brzezinski (2002), Silicic acid leakage from the Southern Ocean as a possible mechanism for explaining glacial atmospheric pCO_2, *Global Biogeochem. Cycles*, *16*(3), 1031, doi:10.1029/2001GB001442.

Matsumoto, K., et al. (2004), Evaluation of ocean carbon cycle models with data-based metrics, *Geophys. Res. Lett.*, *31*, L07303, doi:10.1029/2003GL018970.

McGillicuddy, D. J., and A. R. Robinson (1997), Eddy-induced nutrient supply and new production in the Sargasso Sea, *Deep Sea Res., Part I*, *44*, 1427–1449.

McGillicuddy, D. J., A. R. Robinson, D. A. Siegel, H. W. Jannasch, R. Johnson, T. Dickeys, J. McNeil, A. F. Michaels, and A. H. Knap (1998), New evidence for the impact of mesoscale eddies on biogeochemical cycling in the Sargasso Sea, *Nature*, *394*, 263–266.

Mills, M. M., C. Ridame, M. Davey, J. La Roche, and R. Geider (2004), Iron and phosphorus co-limit nitrogen fixation in the eastern tropical North Atlantic, *Nature*, *429*, 292–294.

Moore, J., S. Doney, J. Kleyplas, D. Glover, and I. Fung (2002a), An intermediate complexity marine ecosystem model for the global domain, *Deep Sea Res., Part II*, *49*, 403–462.

Moore, J., S. Doney, D. Glover, and I. Fung (2002b), Iron cycling and nutrient-limitation patterns in surface waters of the world ocean, *Deep Sea Res., Part II*, *49*, 463–507.

Najjar, R. G., J. L. Sarmiento, and J. R. Toggweiler (1992), Downward transport and fate of organic matter in the ocean: Simulations with a general circulation model, *Global Biogeochem. Cycles*, *6*, 403–462.

Oschlies, A. (2002), Can eddies make ocean deserts bloom, *Global Biogeochem. Cycles*, *16*(4), 1106, doi:10.1029/2001GB001830.

Oschlies, A., and V. Garçon (1998), Eddy-induced enhancement of primary production in a model of the North Atlantic Ocean, *Nature*, *394*, 266–269.

Paltridge, G., and C. Platt (1976), *Radiative Processes in Meteorology and Climatology*, Elsevier, New York.

Parekh, P., M. J. Follows, and E. A. Boyle (2004), Modeling the global ocean iron cycle, *Global Biogeochem. Cycles*, *18*, GB1002, doi:10.1029/2003GB002061.

Parson, T. R., M. Takahashi, and B. Hargrave (1990), *Biological Oceanographic Processes*, 330 pp., Elsevier, New York.

Pelegri, J. L., and G. T. Csanady (1991), Nutrient transport and mixing in the Gulf Stream, *J. Geophys. Res.*, *96*, 2577–2599.

Petit, J. R., et al. (1999), Climate and atmospheric history of the past 42,0000 years from the Vostok ice core, Antarctica, *Nature*, *399*, 429–436.

Pondaven, P., D. Ruiz-Pino, J. N. Druon, C. Fravalo, and P. Tréguer (1999), Factors controlling silicon and nitrogen biogeochemical cycles in the high nutrient, low chlorophyll systems (the Southern Ocean and the North Pacific): Comparison with a mesotrophic system (the North Atlantic), *Deep Sea Res., Part I*, *46*, 1923–1968.

Popova, E. E., V. A. Ryabchenko, and M. J. R. Fasham (2000), Biological pump and vertical mixing in the Southern Ocean: Their impact on atmospheric CO_2, *Global Biogeochem. Cycles*, *14*, 477–498.

Price, N. M., B. A. Ahner, and F. M. M. Morel (1994), The equatorial Pacific Ocean: Grazer-controlled phytoplankton populations in an iron-limited system, *Limnol. Oceanogr.*, *39*, 520–534.

Rhee, G.-Y., and I. J. Gotham (1981), The effect of environmental factors on the phytoplankton growth: Light and the interactions of light with nitrate limitation, *Limnol. Oceanogr.*, *26*, 649–659.

Roe, P. L. (1985), Some contributions to the modeling of discontinuous flows, in *Large-Scale Computations in Fluid Mechanics*, edited by B. E. Engquist, S. Osher, and R. C. J. Somerville, Am. Math. Soc., Providence, R. I.

Rose, A. L., and T. D. Waite (2003), Kinetics of iron complexation by dissolved natural organic matter in coastal waters, *Mar. Chem.*, *84*, 85–103.

Rue, E. L., and K. W. Bruland (1995), Complexation of iron (III) by natural organic ligands in the Central North Pacific as determined by a new competitive ligand equilibration/adsorptive cathodic stripping voltammetric method, *Mar. Chem.*, *50*, 117–138.

Rue, E. L., and K. W. Bruland (1997), The role of organic complexation on ambient iron chemistry in the equatorial Pacific Ocean and the response of a mesoscale iron addition experiment, *Limnol. Oceanogr.*, *42*, 901–910.

Sakshaug, E., and D. Slagstad (1991), Light and productivity of phytoplankton in polar marine ecosystems: A physiological view, *Polar Res.*, *10*, 579–591.

Sañudo-Wilhelmy, S. A., A. B. Kustka, C. J. Gobler, D. A. Hutchins, M. Yang, K. Lwiza, J. Burns, D. G. Capone, J. A. Raven, and E. J. Carpenter (2001), Phosphorus limitation of nitrogen fixation by *Trichodesmium* in the central Atlantic Ocean, *Nature*, *411*, 66–69.

Sarmiento, J. L., N. Gruber, M. A. Brzezinski, and J. P. Dunne (2004), High latitude controls of thermocline nutrients and low latitude biological productivity, *Nature*, *427*, 56–60.

Schlitzer, R. (2002), Carbon export fluxes in the Southern Ocean: results from inverse modeling and comparison with satellite-based estimates, *Deep Sea Res., Part II*, *49*, 1623–1644.

Sunda, W. G. (1997), Control of dissolved iron concentrations in the world ocean: A comment, *Mar. Chem.*, *57*, 169–172.

Sunda, W. G., and S. A. Huntsman (1995), Iron uptake and growth limitation in oceanic and coastal phytoplankton, *Mar. Chem.*, *50*, 189–206.

Sunda, W., D. Swift, and S. Huntsman (1991), Low iron requirement for growth in oceanic phytoplankton, *Nature*, *351*, 55–57.

Tréguer, P., D. M. Nelson, A. J. van Bennekom, D. J. DeMaster, A. Leynart, and B. Queguiner (1995), The silica balance in the world ocean, *Science*, *268*, 375–379.

Trenberth, K., J. Olson, and W. Large (1989), A global wind stress climatology based on ECMWF analyses, *Tech. Rep. NCAR/TN-338+STR*, Natl. Cent. for Atmos. Res., Boulder, Colo.

Usbeck, R., R. Schlitzer, G. Fischer, and G. Wefer (2003), Particle fluxes in the ocean: Comparison of sediment trap data with results from inverse modeling, *J. Mar. Syst.*, *39*, 167–183.

van den Berg, C. (1995), Evidence for organic complexation of iron in seawater, *Mar. Chem.*, *50*, 139–157.

Watson, P., D. C. E. Bakker, A. J. Ridgwell, P. W. Boyd, and C. S. Law (2000), Effect of iron supply on Southern Ocean CO_2 uptake and implications for glacial CO_2, *Nature*, *407*, 730–733.

Williams, R. G., and M. J. Follows (1998), The Ekman transfer of nutrients and maintenance of new production over the North Atlantic, *Deep Sea Res., Part I*, *45*, 461–489.

Williams, R. G., and M. J. Follows (2003), Physical transport of nutrients and the maintenance of biological production, in *Ocean Biogeochemistry: A JGOFS synthesis*, edited by M. Fasham, pp. 19–50, Springer, New York.

Williams, R. G., A. McLaren, and M. J. Follows (2000), Estimating the convective supply of nitrate and implied variability in export production, *Global Biogeochem. Cycles*, *14*, 1299–1313.

Witter, A. E., and G. W. Luther (1998), Variation in Fe-organic complexation with depth in the Northwestern Atlantic Ocean and determined using a kinetic approach, *Mar. Chem.*, *62*, 241–258.

Witter, A., D. Hitchins, A. Butler, and G. Luther (2000), Determination of conditional stability constants and kinetic constants for strong model Fe-binding ligands in seawater, *Mar. Chem.*, *69*, 1–17.

Yamanaka, Y., and E. Tajika (1997), Role of dissolved organic matter in the marine biogeochemical cycle: Studies using and ocean biogeochemical general circulation model, *Global Biogeochem. Cycles*, *11*, 599–612.

S. Dutkiewicz, M. J. Follows, and P. Parekh, Department of Earth, Atmospheric and Planetary Sciences, Massachusetts Institute of Technology, 54-1412, 77 Massachusetts Avenue, Cambridge, MA 02139, USA. (stephd@ocean.mit.edu)

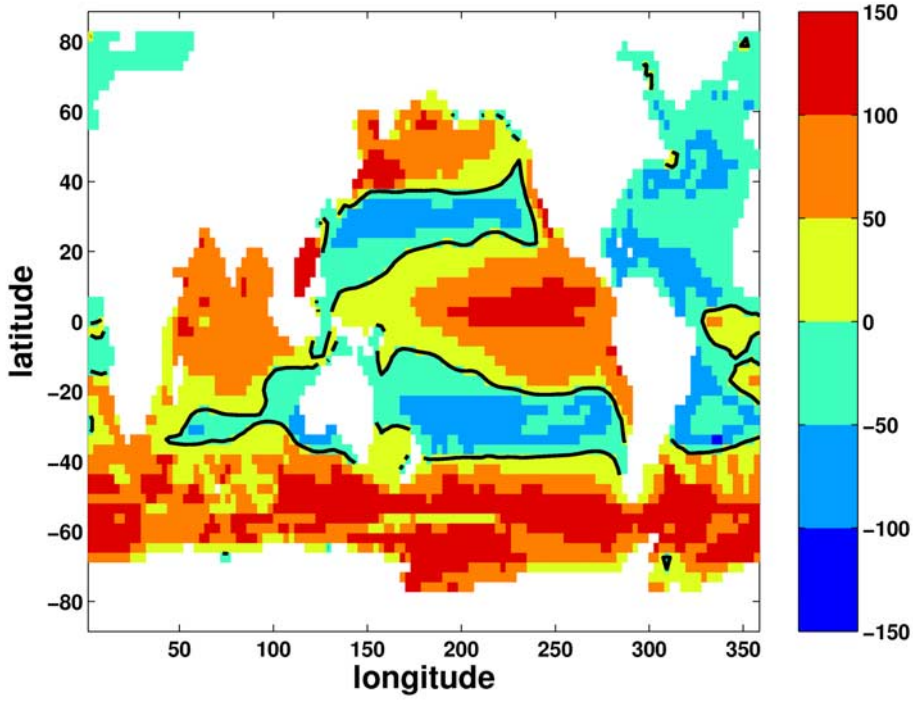

Figure 11. Difference in primary production (gC m^{-2} yr^{-1}) between high and low dust sensitivity studies. Solid line is zero contour. Positive values indicate higher production when aeolian dust supply is enhanced.

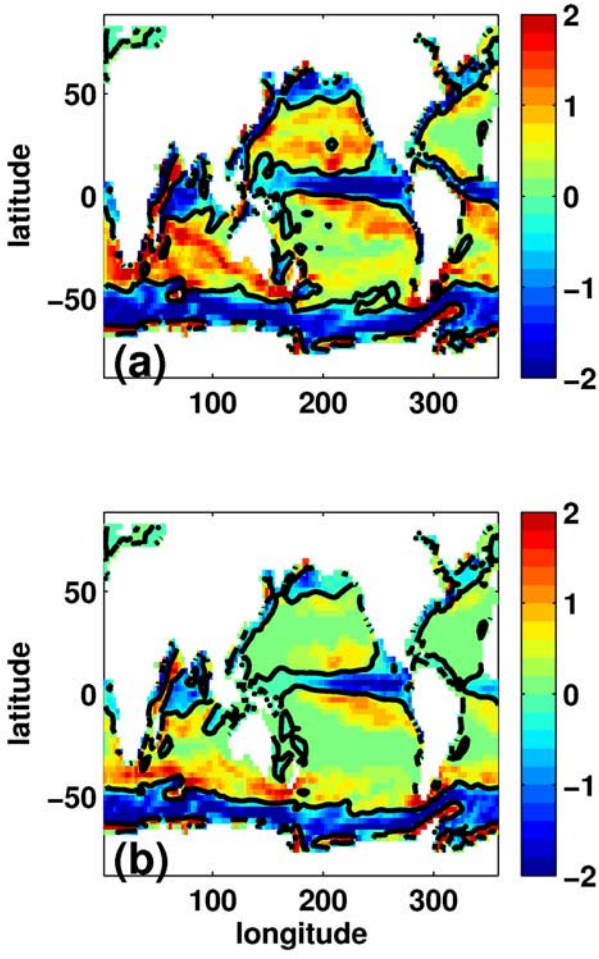

Figure 13. Tendency of phosphate in top layer (0–50 m) of model (μM yr^{-1}) owing to horizontal transport for (a) low and (b) high dust experiments. Negative tendency indicates a net lateral removal of phosphate, and positive indicates a net lateral convergence of phosphate. The advection in this layer is dominated by Ekman dynamics.